Using Rate Transient Analysis and Bayesian Algorithms for Reservoir Characterization in Unconventional Gas Wells during Linear Flow

P. Yuhun, O. O. Awoleke*, and **S. D. Goddard,** University of Alaska

Summary

The main objective of this work is to improve robust, repeatable interpretation of reservoir characteristics using rate transient analysis (RTA). This is to generate probabilistic credible intervals for key reservoir and completion variables. This resulting data-driven algorithm was applied to production data from both synthetic and actual case histories. Synthetic production data from a multistage, hydraulically fractured horizontal completion in a reservoir modeled after the Marcellus Shale reservoir were generated using a reservoir model. The synthetic production data were analyzed using a combination of RTA and Bayesian techniques. First, the traditional log-log plot was produced to identify the linear flow production regime. Using the linear flow production data and traditional RTA equations, Bayesian inversion was carried out using two distinct Bayesian methods. The "rjags" and "EasyABC" packages in the open-source statistical software *R* were used for the traditional and approximate inversion, respectively. Model priors were based on (1) information available about the Marcellus Shale from technical literature and (2) results from a hydraulic fracturing forward model. Posterior distributions and credible intervals were produced for the fracture length, matrix permeability, and skin factor. These credible intervals were then compared with true reservoir and hydraulic fracturing data. The methodology was also repeated for an actual case in the Barnett shale. The most substantial finding was that for nearly all the investigated cases—including complicated scenarios (such as including finite fracture conductivity, fracturing fluid flowback, and heterogeneity in fracture length in the reservoir/hydraulic fracturing forward model)—the combined RTA-Bayesian model provided a 95% credible interval that encompassed the true values of the reservoir/hydraulic fracture parameters. We also found that the choice of the prior distribution did not affect the posterior distribution/credible interval in a significant manner as long as it was moderately concentrated and consistent with engineering science. Also, a comparison of the approximate Bayesian computation (ABC) and the traditional Bayesian algorithms showed that the ABC algorithm reduced computational time by at least an order of magnitude with minimal loss in accuracy. In addition, the production history used, the number of iterations, and the tolerance of fitting in the ABC analysis had a minimal impact on the posterior distribution after an optimal point, which were determined to be at least 1-year production history, 10,000 iterations, and 0.001, respectively. In summary, the RTA-Bayesian production analysis method was implemented using relatively user-friendly computational platforms [*R* and Excel® (Microsoft Corporation, Redmond, Washington, USA)]. This methodology provided reasonable characterization of all key variables such as matrix permeability, fracture length, and skin when compared to results obtained from analytical methods. This probabilistic characterization has the potential to enable better understanding of well performance ranges expected from shale gas wells. The methodology described here can also be generalized to shale oil systems during linear flow.

Introduction

Both pressure transient analysis and RTA are commonly used for reservoir characterization, drainage volume determination, and fracture network characterization. Both techniques are similar in terms of the basic principles, but the duration and accuracy of data measurement are different. Pressure transient analysis takes a short-term event analysis approach that requires carefully controlled input/output conditions. This necessitates the use of precise pressure gauges and accurate flow rate measurements. RTA is more holistic in scope, and the resolution of the gauges can be poorer for RTA compared to pressure transient analysis according to Blasingame (2013). In shale gas reservoirs, the general problem is the ultralow permeability, which greatly increases the time for the pressure pulse to reach the boundary. Sometimes, it can take up to 3 years for the pressure pulse introduced at the wellbore to reach the boundary (Nobakht and Clarkson 2012). This limitation is a major impediment to conducting successful pressure transient analysis tests in low-permeability reservoirs. Instead, production analysis tools such as RTA have become the only viable option. So far, applying RTA principles to the linear flow regime is the basic analytical method that is frequently used because it results in a closed-form solution. It is also relatively simple to apply because a less-comprehensive data set is required for the analysis compared to the reservoir simulation method (Komurcu 2014). In this paper, we used the correction factor for slope errors in the case of high drawdowns during linear flow as proposed by Ibrahim and Wattenbarger (2006). Other nonlinearities such as adsorption and gas slippage effect are not the focus of this work.

Naturally, only numerical solutions to the nonlinear model can fully handle overall hypothesis complexity. Some numerical models have been built with many improvements on grid size and timestep selection to ensure the accuracy of the solution (Komurcu 2014). Recently, Nejadi et al. (2015) characterized fracture parameters using a combination of discrete-fracture-network modeling, dynamic flow responses, a dual porosity model, and an assisted history matching algorithm. They reported success in characterizing the fracture parameters from a multifractured shale well from the Horn River Basin. Moinfar et al. (2016) compared the results from using RTA and numerical simulation for estimated ultimate recovery (EUR) calculations in unconventional shale oil reservoirs. They found that for real life scenarios, the RTA model underpredicted EUR by approximately 6 to 17% compared to the numerical models when a 2-year span of production was used as hindcast. Chen et al. (2016) used parallelized history matching and the randomized maximum likelihood method to generate multiple realizations of the reservoir model. These realizations are conditioned on production data and were

*Corresponding author; email: ooawoleke@alaska.edu

Original SPE manuscript received for review 24 August 2020. Revised manuscript received for review 7 May 2021. Paper (SPE 206711) peer approved 10 May 2021.

used to characterize uncertainties caused by reservoir and hydraulic fracture properties. Their method was also used to history match an example liquid-rich shale reservoir. Khanal et al. (2016) forecasted production from liquid-rich gas condensate reservoirs with multiphase flow using decline-curve analysis, RTA, principal component analysis, and a compositional simulator. They recognized that the more rapid, approximate methods will continue to be used for routine analysis by engineers but emphasized that these relatively simpler methods do not reproduce the forecast from robust reservoir simulation. Wantawin et al. (2017) used high-degree polynomial models to represent a shale gas reservoir simulator. Higher-degree polynomials were used as opposed to quadratic polynomials because they offered the possibility of providing an expanded set of history matching solutions, thereby leading to wider investigation of the range of uncertainty of probabilistic forecasts. This approach was applied to accessing the uncertainty of reservoir and fracture properties in unconventional reservoirs, with a specific example from the Marcellus Shale. De Holanda (2019) presented an extension of the capacitance-resistance model called the second Jacobi theta function model for unconventional reservoirs. Bayesian methodology was used to provide estimates of flow rates and EUR. Based on the results, De Holanda made the claim that the Jacobi model has smaller associated uncertainty and provides more conservative forecasts compared to other commonly used decline-curve analysis models. Sureshjani et al. (2020) coupled an RTA-based analytical equation with Markov Chain Monte Carlo (MCMC). They used their method to estimate two permeability-related parameters and the hydraulic fracture half-length with success.

Of all the reviewed work, only Sureshjani et al. (2020) coupled an RTA-based analytical equation with a Bayesian algorithm. They, however, did not state in their paper how long it took their model to run and did not discuss the convergence characteristics of their posterior distributions either by using trace plots or the scale reduction factor described by Gelman and Rubin (1992) for assessing the degree to which multichain Bayesian algorithms achieve convergence.

The probabilistic approach that we describe in this paper combines the RTA framework with Bayesian statistics. Specifically, after comparing traditional Bayesian methodology to approximate Bayesian methodology using four cases, we focus on applying ABC and RTA for reservoir characterization. Our main contribution is to show that for this specific application, engineers can use RTA-ABC to characterize hydraulically fractured horizontal wells. Further, we give engineers a road map for using this method, and show that this method is more computationally efficient than a simple version of the traditional Bayesian approach for these data sets.

The objectives of this paper are as follows:

1. To combine relatively simple analytical tools of performance prediction and fracture geometry estimation with traditional Bayesian algorithms and ABC.
2. To identify a probabilistic range of predicted reservoir/fracture parameters for relatively simple synthetic cases to reflect the nature of shale/tight gas uncertainties using ABC.
3. To study the impact of different prior distributions on credible intervals.
4. To prove the validity of this new analytical-probabilistic method in more complex reservoir cases.
5. To examine the application of this new method to actual field data.

Methods

Bayesian Methodology Applications. A Bayesian approach was first applied to production data from shale gas reservoirs by Gong et al. (2011). They combined Bayesian methodology with the Arps decline-curve model to quantify uncertainty in reserves estimation, resulting in an uncertainty band for actual production data. Others have also applied Bayesian methodology for reserves forecasting using MCMC algorithms such as Metropolis-Hastings (MH) samplers (Gong et al. 2011), Hamiltonian MCMC algorithms (Goodwin 2012), and ABC (Paryani et al. 2017). Similarly, Yu et al. (2016) paired the fractional decline-curve model with MH. Here, we apply Bayesian methodology to RTA to estimate fracture and reservoir properties from production data. We consider two ways to combine RTA and Bayesian methodology—a traditional likelihood-intensive approach and an ABC approach.

Traditional Bayesian Approach. According to Bayes' theorem, beliefs and uncertainties about model parameters, conditional on observed data and prior beliefs about them, are quantified in the parameters' posterior distribution as given in Eq. 1.

$$\pi(\theta|X) = \frac{l(X|\theta)\pi(\theta)}{\pi(X)}. \quad (1)$$

Here, $\pi(\theta|X)$ is the posterior distribution of parameters θ (which may be a vector), given observed data X; $\pi(\theta)$ is the prior probability distribution of model parameters; $l(X|\theta)$ is a likelihood function; and $\pi(X)$ is constant in θ [and is only included to make $\pi(\theta|X)$ a proper density function]. Although Eq. 1 might theoretically be evaluated directly using multidimensional integration in its denominator, this is usually avoided in favor of stochastic algorithms such as MCMC samplers. These stochastic algorithms sample directly from the posterior distribution under mild regularity conditions, provided the simulation is run long enough.

The MH sampler draws correlated samples from a proposal distribution in such a way that their limiting distribution matches the target posterior distribution $\pi(\theta|X)$. Given a previous draw θ^0 and some designated proposal distribution $Q(\theta|\theta^0)$, a candidate draw from the proposal is taken, which will be denoted as θ^*. The algorithm shapes the distribution of the draws from $Q(\theta|\theta^0)$ into $\pi(\theta|X)$ by only accepting a fraction of them. Each proposed θ^* is accepted with probability equal to the minimum of 1 and $h(\theta^*, \theta^0)$, which is known as the *acceptance ratio* and is defined in Eq. 2.

$$h\left(\theta^*, \theta^0\right) = \frac{l(X|\theta^*)\pi(\theta^*)}{l\left(X|\theta^0\right)\pi\left(\theta^0\right)} \frac{Q\left(\theta^0|\theta^*\right)}{Q\left(\theta^*|\theta^0\right)}. \quad (2)$$

If θ^* is accepted, the algorithm draws a new candidate from the proposal. If it is rejected, the algorithm records θ^0 as an accepted draw for the current step and then draws a new candidate. These steps are repeated over a large number of cycles. A comprehensive discussion of MH as applied to this task can be found in the work of Yuhun (2019).

Approximate Bayesian Computation with MCMC. As described previously, the traditional Bayesian approach requires evaluating a likelihood function to estimate a posterior distribution. The evaluation of the likelihood function can be computationally intensive, even for simple Gaussian likelihoods, as in this study [notably, Gong et al. (2011) also encountered challenges in calculating their likelihood function]. ABC was originally proposed (Pritchard et al. 1999) to eliminate this step, which can significantly reduce computational time (Paryani et al. 2017). The evaluation of the likelihood function in Eq. 1 is replaced with a stochastic simulation model (Hartig et al. 2011) that, over many iterations and when couched inside an MCMC sampler, produces draws from a distribution that approximates the posterior $\pi(\theta|X)$. The advantages of ABC-MCMC over traditional MCMC are most salient for large and complex models (Lintusaari et al. 2017). Paryani et al. (2017) was one of the first works describing ABC methods in the discipline; they applied it to

probabilistic decline-curve analysis. At least three "flavors" of ABC are commonly used: rejection ABC, "Marjoram_original" ABC-MCMC, and "Marjoram" ABC-MCMC.

Rejection ABC draws a candidate parameter value θ^* from the prior distribution of θ and then simulates a sample of data from the likelihood, conditioned on θ^*. The algorithm then either accepts or rejects θ^* depending on whether the simulated data set (or some summary thereof) is similar enough to the original data set (or a summary). The standard for "similar enough" is a distance measure $\omega(X, Y)$, where X and Y represent the original data set (or its summary statistic) and the simulated data set (or its summary statistic), respectively. The function $\omega()$ is preselected by the analyst to quantify the distinctness of pairs of data sets (or summary statistics) and can be something as basic as a simple difference. The algorithm then accepts θ^* if $\omega(X, Y)$ is less than some fixed threshold $\omega_{\max}$. Explanations that provide insight into why this ABC approach works are given by Hartig et al. (2011) and Marjoram et al. (2003).

When "likelihoods are either hard or impossible to calculate" (Marjoram et al. 2003), ABC-MCMC replaces the two likelihood evaluations in Eq. 2 with data simulation in the manner of the rejection algorithm just described. In particular, given a previous draw θ^0 and a candidate θ^* drawn from the proposal distribution $Q(\theta|\theta^0)$, a new sample of data is drawn from the likelihood (conditional on θ^*). Again, let X represent the original data (or its summary statistic) and Y represent the newly-drawn data (or a statistic). If a distance measure $\omega(X, Y)$ falls beneath some threshold $\omega_{\max}$, θ^* can be accepted with a probability equaling the lesser of 1 and $g(\theta^*, \theta^0)$, as given in Eq. 3 (Marjoram et al. 2003). If either $\omega(X, Y) > \omega_{\max}$ or θ^* is not randomly accepted, the algorithm records θ^0 as an accepted draw for the current step and then draws a new candidate.

$$g(\theta^*, \theta^0) = \frac{\pi(\theta^*)}{\pi(\theta^0)} \frac{Q(\theta^0|\theta^*)}{Q(\theta^*|\theta^0)}. \quad (3)$$

Over many iterations, this algorithm draws from the stationary distribution $\pi[\theta|\omega(X, Y)] \le \omega_{\max}$ (Marjoram et al. 2003). This distribution approximates the desired distribution $\pi(\theta|X)$. As with traditional MH sampling, the algorithm's convergence to its target distribution for a given number of iterations is sensitive on the choice of proposal $Q(\theta|\theta^0)$. Our particular choices of $\omega()$, $\omega_{\max}$, summary statistic, and $Q(\theta|\theta^0)$ are given later on, and we discuss the results' sensitivity to these. Throughout, this ABC-MCMC algorithm is termed the "Marjoram_original" version, following the syntax of the "EasyABC" package (Jabot et al. 2015).

After the introduction of ABC-MCMC, researchers found that its chains often do not mix and converge well. In response, Wegmann et al. (2009) developed a variation of "Marjoram_original" ABC-MCMC, which was partially implemented in "EasyABC" as the Marjoram algorithm. This algorithm starts with a calibration period of, for example, 10,000 iterations, during which the algorithm can roughly estimate the sampling distribution of $\pi(\omega|X, \theta)$, which is influenced by both $l(Y|\theta)$ and $\pi(\theta)$. The calibration period aims to inform the selection of a value for $\omega_{\max}$. Because the arbitrary choice of $\omega_{\max}$ runs the risk of being too large (which would undermine the quality of the algorithm's approximation of the target posterior) or being too small (which could force the algorithm to unnecessarily reject too many draws of θ^*), any information for determining the best $\omega_{\max 1}$ is valuable. The algorithm then picks its own $\omega_{\max}$ by taking the τth percentile of the estimated distribution of $\pi(\omega|X, \theta)$. The user-supplied value of τ is known as the *tolerance* and should be relatively small. The calibration period is also used for tuning the proposal distribution $Q(\theta|\theta^0)$. Ideally, this allows the chain to explore the whole space of possible values of θ while staying mainly concentrated on regions where the acceptance rate of proposed θ^*s is high. Thus, this calibration period seeks to strike an optimal balance between effective mixing and computational efficiency.

In addition, Marjoram ABC-MCMC performs a local-linear regression to adjust accepted draws of θ so that a somewhat-larger tolerance τ can be set, while the algorithm still yields posterior distributions that are approximately correct. This approach was introduced by Beaumont et al. (2002). Marjoram ABC-MCMC is used hereafter because it requires less computational time.

RTA with Bayesian Methodology. In the RTA-Bayesian method, the procedure is analogous to the conventional RTA process in gas shales, especially with regard to the flow regime characterization process. Two plots are critical for shale gas production analysis: the log-log plot and the specialized plot (square root of time plot). We note that it is important to filter out all noise in production data that may occur as a result of operational issues or liquid loading. This is because these kinds of erroneous data can lead to misleading interpretations when characterizing the flow regime (Anderson et al. 2010).

Our method begins with the generation of synthetic production data from a reservoir simulator. The log-log plot is constructed to identify linear flow regime. The related production data are analyzed with our methods. We use prior distributions—which represent our present knowledge about the system—and the synthetic data to sample from the posterior distributions using both traditional and approximate Bayesian methods. Trace plots and density plots are constructed to evaluate convergence. Next, the probabilistic results from our method are compared with the input variables from the reservoir simulator, including x_f, k_m, n_f, and s. Parameter x_f is the fracture half-length (ft, L), k_m is the matrix permeability (md, L^2), n_f is the number of hydraulic fractures (dimensionless), and s is the skin factor (dimensionless). As discussed later, this analysis procedure is applied to a variety of test cases that range from simple to complicated. However, before discussing the test cases, we further describe the method in the following discussion.

Step 1—Generation of Synthetic Production Data. In this study, the synthetic production data are generated with the help of a commercial simulator. The multistage horizontal well completion with hydraulic fracturing, depicted in **Fig. 1,** is modeled using an industry-standard reservoir simulator. The reservoir properties to build the model are based on those of Marcellus Shale, which are presented in **Table 1.** A constant wellbore flowing pressure (200 psi) was used. Moreover, a 20-year simulation period is used to ensure that the production data are sufficient for the analysis. This also ensures that the simulation period will encompass the linear flow regime, which tends to be of the longest duration in ultralow-permeability reservoirs. Using synthetic production data from a "known" reservoir model will help in the validation of the RTA-Bayesian methodology: If the actual values of variables like fracture half-length, matrix permeability, and skin fall in the credible interval calculated using the RTA-Bayesian methodology for a number of synthetic test cases, we might consider this methodology to be validated for relatively simple cases.

Step 2—Identification of Linear Flow Regime Using the Log-Log Derivative Plot. The linear or bilinear flow portion of the synthetic production data is identified using the traditional log-log rate normalized pressure (RNP) and RNP derivative plots. The objective of the latter is to identify the period that is dominated by linear flow, whether from early or late transient linear flow. The early linear flow occurs when flow from formation enters the fracture with no interference from the other fractures. The late transient linear flow occurs when flow from the outermost regions of the matrix enters the whole fracture system. The linear flow region is marked by a unit slope on a log-log plot between RNP (or RNP derivative) and square root of time.

Step 3—Imposition of Prior Distributions and Likelihood Function. Both the Bayesian approaches described previously require prior distributions to be imposed on model parameters, and both require likelihood functions to be assumed to invert the synthetic production data. Below we discuss these distributional assumptions in detail.

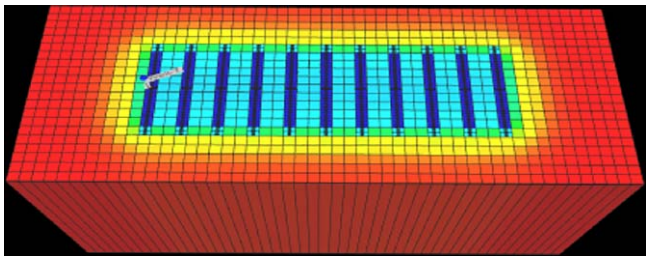

Fig. 1—Reservoir model for hydraulically fractured horizontal well.

Model Properties (units, dimensions)	Value
Reservoir thickness (ft, L)	150
Effective porosity (fraction, dimensionless)	0.1
Gas gravity (fraction, dimensionless)	0.56 to 0.62
Formation compressibility (psi^{-1}, $m^{-1}Lt^2$)	5.00×10^{-6}
Water compressibility (psi^{-1}, $m^{-1}Lt^2$)	3.40×10^{-6}
Reservoir pressure (psi, $mL^{-1}t^{-2}$)	2,000
Reservoir temperature (°F, T)	220
Matrix permeability (md, L^2)	0.00013 to 0.006

Table 1—Synthetic model properties in reference to Marcellus Shale reservoir (Zagorski et al. 2012).

RTA with Traditional Bayesian Methodology. The priors of unknown model parameters (x_f, k, s) are based on knowledge such as information from core samples and/or engineering designs such as the designed fracture half-length for hydraulic fracturing. The use of informative prior distributions can help reduce computational time and aid in the convergence of results. In this work, most of the prior distributions are assumed to be uniform. This ensures that all the prior values within the bounds of the distribution are considered equally likely, a priori. The rationale concentrates inferences on the information contained in the data (production, pressure, and/or gas potential) themselves. The RTA constant pressure and superposition solutions for gas wells during linear flow can be found in Eqs. 4 and 7, respectively. Eq. 4 is from Bello and Wattenbarger (2010) with a correction for high pressure drawdown f_{cp} from Ibrahim and Wattenbarger (2006; see Eqs. 5 and 6). The errors (ε) account for the difference between the observed data and the simulated data; their distribution is discussed below. The definition of A_c is shown in Eq. 9. Eqs. 4, 5, and 6 are used for all cases run except the field case, for which Eq. 7 is used.

$$\mu_m = \frac{m(p_i)-m(p_{wf})}{q} = f_{cp}\frac{1{,}262T}{\sqrt{k_m(\phi\mu c_t)_i}A_c}\sqrt{t}+\frac{1{,}424Ts}{\sqrt{A_c}k_m}\left[\frac{2\pi}{1+\frac{0.8}{s}\sqrt{\frac{0.00633k_mt}{(\phi\mu c_t)_iA_c}}}\right]+\varepsilon. \quad \ldots\ldots (4)$$

$$f_{cp} = 1-0.0852D_D-0.0857D_D^2. \quad \ldots\ldots (5)$$

$$D_D = \frac{m(p_i)-m(p_{wf})}{m(p_i)}. \quad \ldots\ldots (6)$$

$$\mu_m = \frac{m(p_i)-m(p_{wf})}{q_n} = \frac{803.2T}{\sqrt{k_m(\phi\mu c_t)_i}A_c}\sum_{j=1}^{n}\frac{q_j-q_{j-1}}{q_n}\sqrt{t_n-t_{j-1}}+\frac{(2\pi)1,424Ts}{\sqrt{A_c}k_m}+\varepsilon. \quad \ldots\ldots (7)$$

$$l(\varepsilon|\sigma^2) = \sqrt{2\pi\sigma^2}e^{-\frac{\varepsilon^2}{2\sigma^2}}. \quad \ldots\ldots (8)$$

$$A_c = (4x_fh)n_f. \quad \ldots\ldots (9)$$

In Eqs. 4 through 9, μ_m is the RNP from the numerical simulator $\left(\frac{psi^2\text{-D}}{cp\text{-}Mscf^2}, mL^{-7}t^{-5}\right)$; D_D is the dimensionless drawdown; $m(p_i)$ is the initial gas pseudopressure $\left(\frac{psi^2\text{-D}}{cp\text{-}Mscf}, mL^{-4}t^{-4}\right)$; $m(p_{wf})$ is the bottomhole flowing gas pseudopressure $\left(\frac{psi^2\text{-D}}{cp\text{-}Mscf}, mL^{-4}t^{-4}\right)$; q is the gas-flow rate $\left(Mscf/D, \frac{L^3}{t}\right)$; q_n is the last recorded gas-flow rate, which should be nonzero $\left(Mscf/D, \frac{L^3}{t}\right)$; q_j is the gas-flow rate at time j $\left(Mscf/D, \frac{L^3}{t}\right)$; T is the reservoir temperature (°F, T); s is the skin factor (dimensionless); subscript i anywhere implies initial reservoir conditions; k_m is the matrix permeability (md, L^2); ϕ is the reservoir porosity (dimensionless); μ is the gas viscosity $(cp, mL^{-1}t^{-1})$; c_t is the total compressibility $(psi^{-1}, m^{-1}Lt^2)$; A_c is the cross-sectional area perpendicular to flow (ft^2, L^2); f_{cp} is a correction factor; x_f is the fracture half-length (ft, L); h is the reservoir thickness (ft, L); n_f is the number of fractures (dimensionless); and ε is the aleatory error.

Regardless of what might be an appropriate distributional assumption for RNP itself, the errors ε might appropriately be assumed to be Gaussian, as is common in classical nonlinear regression analysis (Maria 2004; Guseo and Dalla Valle 2005). This assumption, denoted as $l()$ in Eq. 8 (to emphasize that this is a likelihood function) is further assumed to have mean 0 and a variance σ^2. The likelihood function and prior distributions (with hyperparameters suppressed) are summarized in **Tables 2 and 3** and discussed further below; in the traditional Bayesian method, the log likelihood was used, and the reported priors were applied to the natural logarithm of the parameters k_m and x_f to prevent numerical underflow problems. A simplified flow chart of RTA with the traditional Bayesian method can be found in **Fig. 2** (left).

Function	Traditional Bayesian Method	ABC Method
Prior distribution	$x_f \sim N(-,-)$ $k_m \sim U(-,-)$ $s \sim U(-,-)$ $\sigma \sim U(-,-)$	$x_f \sim N(-,-)$ $k_m \sim U(-,-)$ $s \sim U(-,-)$
Likelihood function	$\varepsilon \sim N(0,\sigma^2)$	$\varepsilon \sim N(0,\sigma^2)$

Table 2—Prior and likelihood function of the traditional Bayesian vs. ABC methods.

Parameters	Prior Distribution	Value
k_m	Uniform	$U(0.0001,\ 0.006)$
x_f	Normal	$N(500, 10^2)$ or $N(900, 10^2)$
s	Uniform	$U(-10,\ 10)$
n_f	Fixed value	5 or 11

Table 3—Prior distributions for parameters in this study.

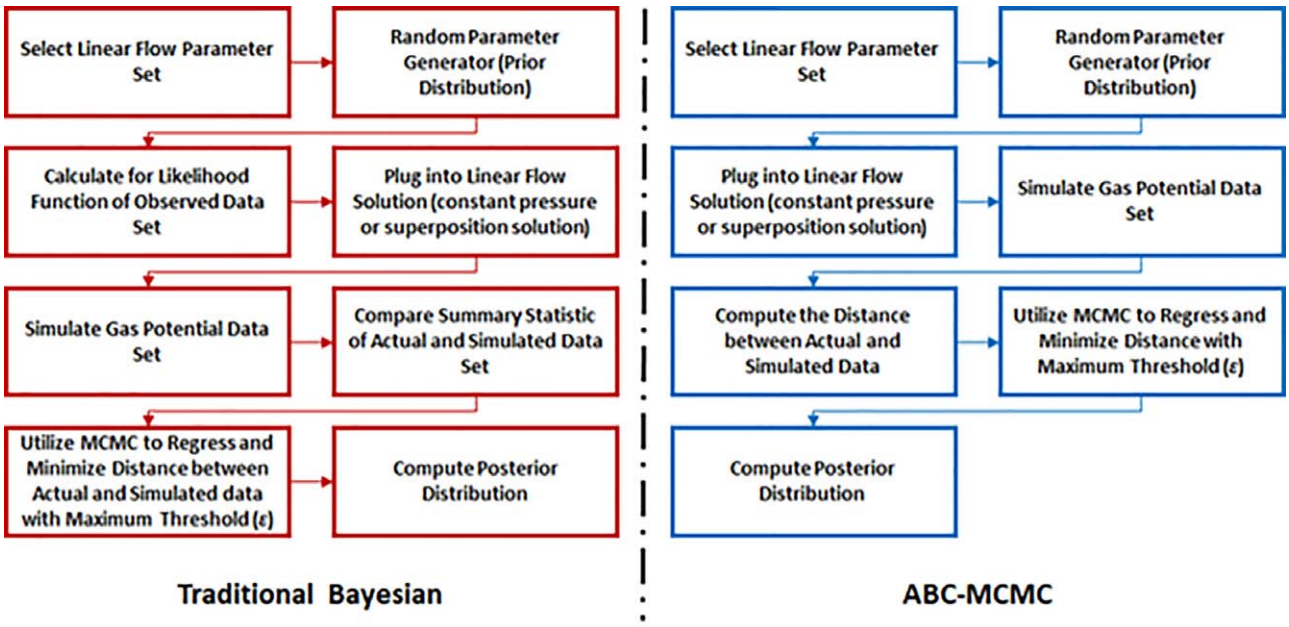

Fig. 2—Flow diagram for traditional Bayesian (left) and ABC-MCMC (right).

It is also possible to set up the problem differently by attempting to estimate the combined parameter $x_f\sqrt{k_m}$. However, in this work we specifically wanted to see whether we could estimate x_f and k_m marginally, especially because we are operating in the production data analysis paradigm. The marginal posterior of x_f obtained is not conditional on $\sqrt{k_m}$ and vice versa (for both traditional Bayesian and ABC-MCMC). It is merely what remains of the joint posterior after all other parameters are integrated. Therefore, assuming convergence has been achieved in the draws from the joint posterior, there is no reason to believe that the algorithm has failed to fully explore any one parameter's marginal distribution, because this may be of concern to some readers. For the test scenarios that will be described later, we focus on presenting the marginal posteriors of all parameters. However, for the field case, we present the marginal posteriors of x_f and k_m as well as that of the combined parameter $(x_f\sqrt{k_m})$.

The traditional Bayesian algorithm was fit using *R* (R Core Team 2020) with the "rjags" package (Plummer 2019). This package implements a Gibbs sampler, which means that the proposal distribution being used for each parameter is approximately a full conditional distribution.

RTA with ABC-MCMC Methodology. The workflow for the ABC-MCMC method is similar to the traditional Bayesian method, except that in the ABC-MCMC methodology, the computation of the likelihood function is not required. Instead, errors are drawn from the likelihood function in Eq. 8 and are incorporated into Eq. 4 or 7 to produce stochastically simulated RNP values. The criteria for choosing the prior distributions for the parameters (x_f, k_m, s) in the ABC-MCMC methodology are the same as for the traditional Bayesian methodology. These priors are mostly assumed to be either Gaussian or uniform (see Test Scenario 1 below for a sensitivity analysis on the shape and spread of priors). The prior distribution of unknown parameters for the linear flow regime in both the constant pressure solution and superposition solution are plugged into Eqs. 1 and 2, respectively, with A_c as defined in Eq. 9. The simulated gas potentials are computed and generated. ABC-MCMC was performed using the package "EasyABC" (Jabot et al. 2015) in R. As described previously, ABC-MCMC computes a distance between raw data and stochastically simulated data when evaluating proposed parameter draws for acceptance. Our implementation used Euclidean distance between vectors of data as the distance function $\omega()$. For the four scenarios below, the Marjoram ABC-MCMC method was used with a tolerance τ set at 0.001. For proposal distributions, the function used uniform distributions of which lower and upper limits are automatically selected after the calibration period, as described previously.

In the Results section, we will evaluate the estimation accuracy of the ABC-MCMC posterior approximations by summarizing them with 95% credible intervals of x_f, k_m, and s and point estimates of the parameters corresponding to the posterior median (P50). A simplified flow chart for RTA with ABC-MCMC can be found in Fig. 2 (right).

In Step 4, reservoir/completion properties are characterized by combining production data and RTA using the Bayesian framework. Finally, Step 5 comprises ascertaining whether the true values lie in the 95% credible interval. Steps 4 and 5 are further illustrated while discussing Scenario 1 later on in this work.

Results

Comparison between Traditional Bayesian and ABC Methodology. In this section, traditional Bayesian and ABC-MCMC methods were used on a variety of initial cases. This was to evaluate the suitability of these methods for RTA. Synthetic production data corresponding to the linear flow regime are identified using the log-log plot and served as the input for the RTA-Bayesian methods. Next, the prior distribution of reservoir parameters such as k_m, x_f, and s are assumed based on prior knowledge as shown in Table 3. The parameters s, x_f, and k_m are assumed to be a priori independent. Matrix permeability is assigned a uniform distribution bounded between 0.0001 and 0.006 md, based on the literature review of Marcellus Shale properties by Zagorski et al. (2012). Skin parameter s is assigned a uniform distribution with a range from −10 to 10 because we know of almost no general prior knowledge about skin factor. There is also a paucity in technical literature about the appropriate skin factor ranges for multistage hydraulically fractured wells. Given that our synthetic examples and the field case had actual skin factors close to zero, we think this skin factor range is appropriate. Fracture half-length (x_f) is assigned a normal distribution with the mean value from the designed fracture half-length (the designed fracture half-length is assumed to be known from fracture modeling studies) and a standard deviation of 10 ft. The prior fracture half-length value can, in practice, be as low as 0 ft or as high as 1,500 ft, but we assumed that these scenarios have very low probability.

In the traditional Bayes method, the parameter σ represents the standard deviation of the errors (meaning the discrepancies between the RNP of the numerical simulator and that of the analytical model). We regard these errors as random variables, even though they may be ultimately traceable to deterministic and complex misalignments between the numerical and analytical models. As the standard deviation of such errors, σ is regarded as a nuisance parameter, and we will refrain from emphasizing the interpretation of its posterior hereafter. For the same reason, we see its prior specification as uncritical as long as that prior reflects our dearth of information about σ's likely value and does not appear to cause convergence or mixing problems. It was assigned a uniform distribution with endpoints at 0 and 100,000 to provide vague prior information.

Next, both the traditional Bayesian and ABC methods were used to generate the posterior distributions of reservoir parameters. A comparison of the algorithms in terms of the number of iterations and computational time is shown in **Table 4** using four simulation cases (Cases A-1 to A-4). Where reporting results of the traditional Bayesian method, values of $\hat{R}$ represent upper confidence limits on the scale reduction factor described by Gelman and Rubin (1992) for assessing the degree to which the algorithm achieved convergence. Values materially larger than 1 constitute evidence against convergence.

					Traditional Bayesian Method						ABC Method				
	Input Parameters						CPU* Time	95% Credible Interval				CPU Time	95% Credible Interval		
Case	k_m (md)	x_f (ft)	n_f	s	Iterations	$\hat{R}$	(min)	k_m (md)	x_f (ft)	s	Iterations	(min)	k_m (md)	x_f (ft)	s
A-1	0.005	500	5	0	10^6	1.31	8.17	0.0004, 0.0049	566, 2,088	−0.013, 0.0004	10^3	0.04	0.0013, 0.0054	367, 965	−0.07, 0.17
A-2	0.0005	500	5	0	10^6	5.67	21.25	0.0002, 0.003	219, 804	0.002, 0.014	10^4	0.3	0.0004, 0.0015	320, 685	−0.11, 0.08
A-3	0.005	900	5	0	10^6	1.01	4.38	0.0009, 0.005	947, 2,219	−0.014, 0.000	10^4	0.27	0.0022, 0.0059	631, 970	−0.04, 0.03
A-4	0.0005	900	5	0	10^6	4.06	73.73	0.0017, 0.0048	324, 692	0.061, 0.193	10^4	0.38	0.0004, 0.0015	811, 1,213	0.13, 0.70

*CPU = central processing unit

Table 4—Comparison results between traditional Bayesian and ABC methods.

For the traditional Bayesian algorithm, three independent chains were simulated with overdispersed initial values of s, x_f, and k_m. In two of the cases, the algorithm did not approximately converge after more than 1 million iterations. For these examples to achieve convergence, the number of iterations may have to exceed 10 million. In general, this dependence on long sampling chains is impractical because of computational time. Therefore, we conclude that a basic MCMC algorithm is not an efficient nor a generally prescriptive approach to solving the problems defined in this study. We realize an argument could be made that the reason why convergence was not achieved in these two examples is because we did not tune the MCMC algorithm parameters properly. Although this is not inconceivable, we contend that for petroleum engineers who may not be expert in every nuance of Bayesian implementation, ABC offers a plausible alternative.

Other diagnostics of the traditional Bayesian method provided little evidence that the model's assumptions were invalid. In particular, the residuals from the four case studies defined in Table 4 generally displayed tail behavior consistent with the normal distribution—in every case they remained within three standard deviations of their mean.

In Table 4, the ABC method is reported to require a much shorter computation time and fewer iterations to attain convergence in all four synthetic production data cases. Specifically, it took less than a minute to sample from the approximate posterior distributions. The traditional Bayesian method took between 4 and 73 minutes, depending on the number of data points and reservoir complexity. All the computations were done on a common desktop computer. We know of no metric for assessing algorithm convergence in ABC-MCMC analogous to the $\hat{R}$ reported in Table 4 for the traditional MCMC. **Fig. 3** shows the trace plots for s, matrix permeability, and fracture half-length for ABC-MCMC (for Case A-1). With the possible borderline exception of x_f, we believe these plots demonstrate no concerning inadequacies in convergence. Trace plots for Cases A-2 to A-4 show similar behavior, but we omit them to conserve space. The 95% credible intervals of the variables reported in Table 4 are in the ballpark compared with the reservoir model input parameters. Thus, the results have so far demonstrated that the ABC method can accurately characterize reservoir/fracture properties. For instance, the calculated probabilistic true value ranges of Case A-1 in Table 4 are $k_m \in (0.0013, 0.0054$ md), $x_f \in (367, 965)$, and $s \in (-0.07, 0.17)$, respectively. Also, **Fig. 4** shows a comparison of the RNP produced from the reservoir simulator compared with the credible interval from the RTA-ABC methodology for Cases A-1 to A-4. The data presented in Fig. 4 are from the linear flow regime. We see that there is a good match between RNP predicted (RTA-ABC) and RTA observed (from reservoir simulator).

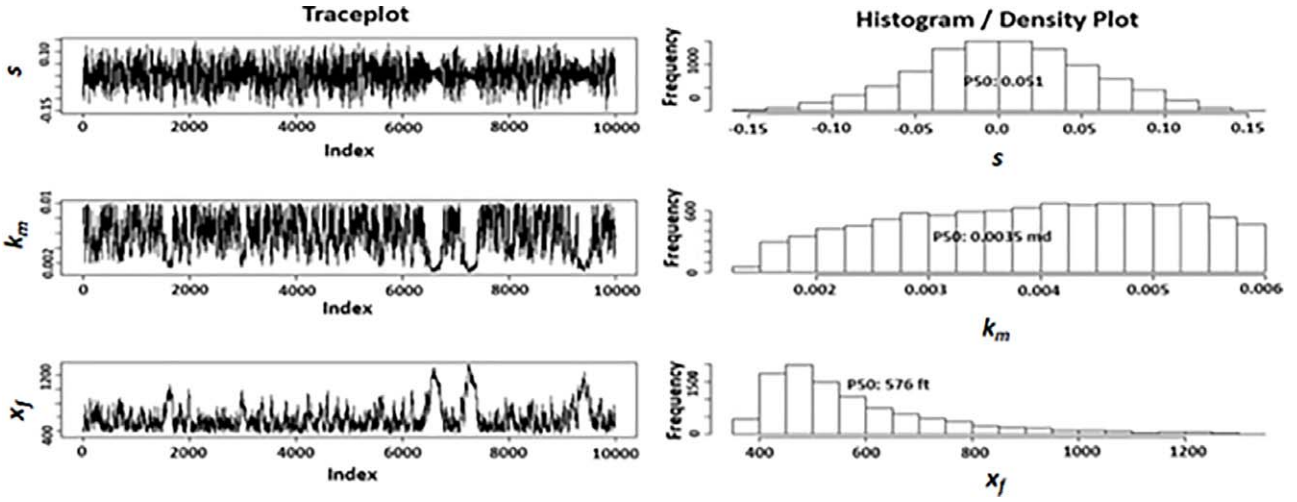

Fig. 3—Case A-1 ABC trace plot for posterior distribution [prior $x_f \sim$N(500,100)].

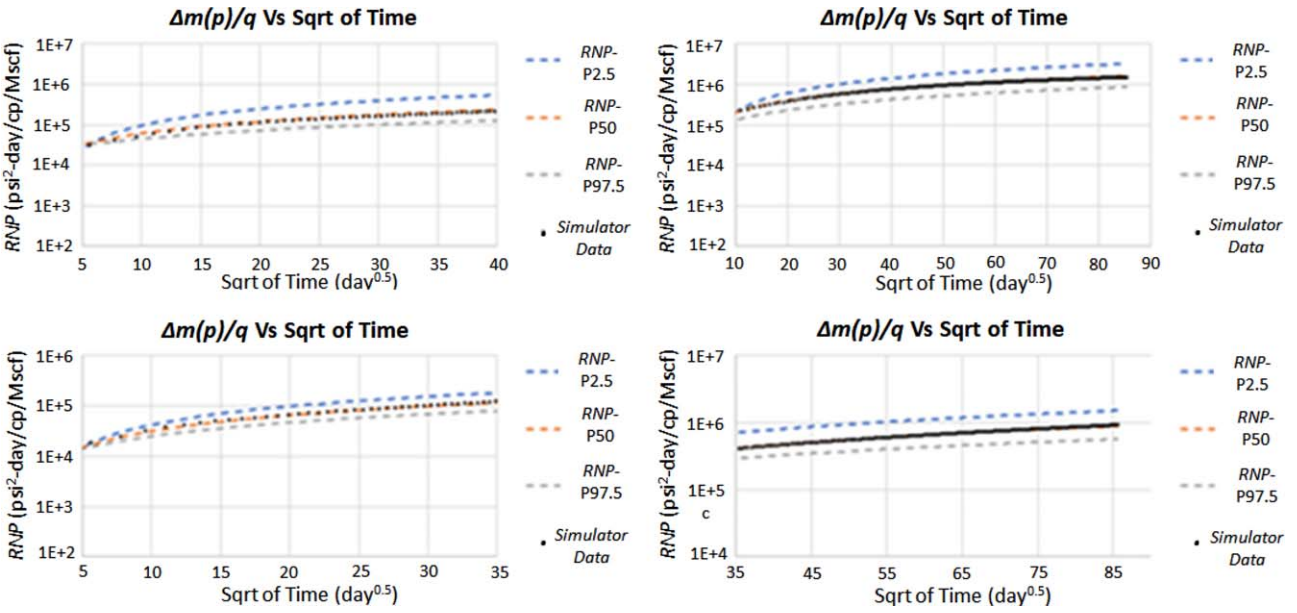

Fig. 4—*RNP* observed vs. *RNP* predicted (linear flow regime data only) for Case A-1 (top left), Case A-2 (top right), Case A-3 (bottom left), and Case A-4 (bottom right). Sqrt = square root.

Test Scenarios. In this study, four scenarios have been attempted using the reservoir simulator to investigate the feasibility of using the methodology described in the previous section; that is, the RTA with ABC method. Each test scenario provides synthetic production data that we will use to show the utility of the RTA-Bayesian method for characterizing reservoir properties or well completion parameters in tight/shale gas reservoirs. In addition, we note that the total skin is not varied but defaulted as 0 in this study for all scenarios.

This is because it was challenging to impose fracture damage skin factor, as well as choked skin factor, in the reservoir model. Scenario 1 (base case study) was designed to validate the study methodology in a simple homogeneous reservoir. Sensitivity runs on major variables such as matrix permeability, fracture half-length, and number of induced hydraulic fractures were performed to validate the RTA-ABC method. Scenario 2 was designed to examine the effect of hydraulic fracture fluid on the estimation accuracy of the RTA-ABC method. This flowback mostly happens during the initial stage of production. Scenarios 3 and 4 were designed to investigate the influence of finite fracture conductivity and fracture half-length heterogeneity on estimation accuracy from the methodology, respectively. The details of these test scenarios are given in **Table 5.** The results for Scenario 1 are presented more comprehensively to illustrate study methodology, whereas concise summaries of the other scenarios are presented. We note here that we did not add noise to these test scenarios. The field case (discussed later), however, naturally did contain random noise.

Topic to Investigate	Generated Case	Matrix Permeability, k_m (md)	Fracture Half-Length, x_f (ft)	Number of Fractures, n_f	Fracture Permeability, k_f (md)	s
Validation of study methodology (RTA-ABC) in a simple homogeneous reservoir (base case)	Case 1.1	0.005	500	5	Infinite	0
	Case 1.2	0.0005	500	5	Infinite	0
	Case 1.3	0.005	900	5	Infinite	0
	Case 1.4	0.0005	900	5	Infinite	0
	Case 1.5	0.005	500	11	Infinite	0
	Case 1.6	0.0005	500	11	Infinite	0
	Case 1.7	0.005	900	11	Infinite	0
	Case 1.8	0.0005	900	11	Infinite	0
Investigate impact of hydraulic fracturing fluid on prediction precision of the RTA-ABC methodology	Case 2.1	0.005	500	5	Infinite	0
	Case 2.2	0.0005	500	5	Infinite	0
	Case 2.3	0.005	900	5	Infinite	0
	Case 2.4	0.0005	900	5	Infinite	0
Investigate impact of finite fracture conductivity on the prediction precision of the RTA-ABC methodology	Case 3.1	0.0005	500	5	Finite 1-3-5 with 1.5 md	0
	Case 3.2	0.0005	500	5	Finite 2-4 with 1.5 md	0
	Case 3.3	0.0005	900	5	Finite 1-3-5 with 1.5 md	0
	Case 3.4	0.0005	900	5	Finite 2-4 with 1.5 md	0
Investigate impact of x_f heterogeneity on the prediction precision of the RTA-ABC methodology	Case 4.1	0.0005	900 and 500	3 and 2	Infinite	0
	Case 4.2	0.0005	900 and 500	2 and 3	Infinite	0
	Case 4.3	0.0005	900 and 500	3 and 2	Finite, $x_f = 500$ ft with 1.5 md	0
Investigate impact of x_f heterogeneity on the prediction precision of the RTA-ABC methodology	Case 4.4	0.0005	900 and 500	3 and 2	Finite, $x_f = 900$ ft with 1.5 md	0

Table 5—Test scenarios.

Scenario 1—Validation of Study Methodology in a Simple Homogeneous Reservoir (Base Case). To verify the robustness of the RTA-Bayesian (ABC) method, the eight cases of synthetic production data during the linear flow regime from the reservoir model (Scenario 1 of Table 5) are simulated with the RTA-Bayesian (ABC) methodology This was to make a comparison between the calculated wellbore/reservoir parameters and reservoir model input (true values). The synthetic production data are generated for 20 years to ensure that the linear flow regime duration is sufficient for the RTA-Bayesian (ABC) methodology. The prior distributions of each of the model parameters are set up to assume weak prior information, as shown in Table 3. The prior distribution of matrix permeability, for example, imposes the lower and upper bounds based on prior knowledge from a literature review of Marcellus Shale properties. Using the RTA-Bayesian (ABC) methodology as shown in Fig. 2 (right), MCMC chains of skin, fracture half-length, and matrix permeability are run with 10,000 iterations to determine the posterior distribution of reservoir/fracture parameters. 10,000 iterations were chosen because they have been observed to be the minimum iteration number required to attain convergence according to Table 4. At the end of the process, the 95% credible intervals (P2.5 to P97.5), which are estimated from posterior distribution of these three parameters, reflect the probabilistic range of estimated reservoir/fracture parameters. After running 10,000 iterations with a residuals tolerance of 0.001, the posterior distribution of three model parameters is generated, and the results are summarized in **Table 6.** Note that in Table 6, the number of fractures in the model is not inferred from the data. It is an input into the reservoir model and varies between 5 and 11. We also note here that hydraulically fractured completions in shale reservoirs now tend to have more fracture stages, but this has historically not always been the case. Even if we accept the argument that the methodology described in this work is not suitable for such cases, it will certainly be useful for completions completed earlier on in the shale revolution. The fracture spacing is 706 ft for the 5-fracture stage completions and 235 ft for the 11-fracture stage completions. The lateral length is 3,000 ft.

				Base Case to Vary k_m, x_f, and n_f								
				k_m – Posterior Distribution (md)			x_f – Posterior Distribution (ft)			s – Posterior Distribution		
Scenario 1	k_m (md)	x_f (ft)	n_f	P2.5	P50	P97.5	P2.5	P50	P97.5	P2.5	P50	P97.5
Case 1.1	0.005	500	5	0.0013	0.0035	0.0054	367	577	965	−0.10	0.02	0.17
Case 1.2	0.0005	500	5	0.0004	0.0009	0.0014	320	462	685	−0.11	0.03	0.16
Case 1.3	0.005	900	5	0.0022	0.0042	0.0059	631	757	970	−0.04	−0.01	0.03
Case 1.4	0.0005	900	5	0.0004	0.0008	0.0015	811	978	1,213	−0.08	0.13	0.70
Case 1.5	0.005	500	11	0.0016	0.0041	0.0058	280	427	617	−0.06	−0.03	0.04
Case 1.6	0.0005	500	11	0.0002	0.0005	0.0017	386	708	866	0.01	0.17	0.65
Case 1.7	0.005	900	11	0.0011	0.0033	0.0058	581	836	1,226	−0.04	−0.01	0.04
Case 1.8	0.0005	900	11	0.0003	0.0015	0.0040	538	821	977	0.00	0.21	0.74

Table 6—95% credible intervals of model parameters in Scenario 1 of Table 5.

The trace plots of each model parameter are shown in **Figs. 5 and 6.** The individual trace plots are mostly spread randomly around a mean value. This observation is a possible sign of convergence. The even cases of Scenario 1 represent the ultralow permeability at 0.0005 md, and the odd cases of Scenario 1 represent the high permeability case at 0.005 md. The trace plots, especially for fracture half-length, are sometimes trapped in a certain region of the model parameter space. This can cause the uncertainties in the prediction of our model parameters. However, the trapping of the trace plots does not seem to affect the histogram/density plot, as observed from the smooth density distribution plot (single mode) in Figs. 5 and 6. Only Cases 1.4 and 1.7 have two humps in their density distributions. When the iteration number is increased to 100,000, the signature of two humps in the density distributions still existed in both Cases 1.4 and 1.7. The model parameters of skin, matrix permeability, and fracture half-length exist within the interval of −0.2 to 0.8, 0.0002 to 0.006 md, and 200 to 1,300 ft, respectively, in all the eight cases. Thus, the predicted results of our model parameters are in the ballpark for all cases. The 95% credible interval of model parameters are determined from each posterior distribution (P2.5-P50-P97.5). Overall, the RTA-Bayesian (ABC) method is confirmed to be useful for completion/reservoir characterization. It also provides a decent accuracy of model parameter prediction when compared with the true values.

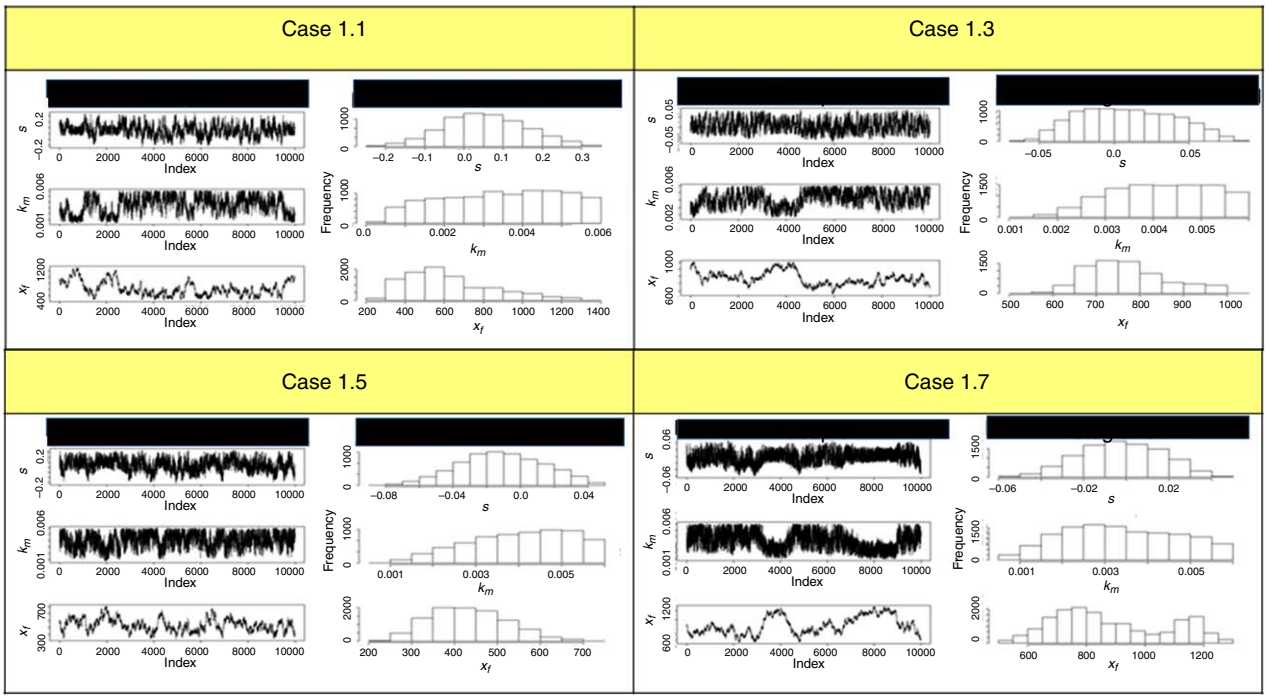

Fig. 5—ABC traceplot and histogram/density plot of odd cases, Scenario 1 (number of iterations = 10,000).

The analysis so far does not include a sensitivity analysis on how the results might be affected by:

1. Using varying amounts of production history.
2. Varying our choice of prior distributions.
3. Changing the number of MCMC iterations.
4. The tolerance τ used by the Marjoram algorithm for setting $\omega_{\max}$.

We now turn our attention to these sensitivity analyses.

Sensitivity to Amount of Production History Used. To clearly understand the impact of production time on the RTA-Bayesian method, Case 1.2 (Table 6), which is ultralow permeability at 0.0005 md, is selected to do sensitivity analysis. A lower-permeability scenario was chosen because boundary effects are observed later when compared to higher-permeability scenarios. A log-log plot of the

data was made to determine the linear flow regime. There was no distinct linear flow regime for the 1-year production case as seen in **Table 7 and Fig. 7.** The last few data points in the 1-year log-log plot could be construed as representing linear flow as shown below. However, we decided not to base analysis on a small set of data points because of the potential for error. The linear flow regime is observed in the other cases of Table 7, and Table 7 also demonstrates that the linear flow regime can be sufficiently identified for RTA with Bayesian (ABC) analysis with at least 2 years of production history for this particular case study. The calculated probabilistic ranges are roughly $k_m \in (0.0002 \text{ md}, 0.001 \text{ md})$, $x_f \in (363, 848)$, and $s \in (-0.07, 0.18)$ respectively. In addition, Table 7 also shows that, for parameters k_m and s, there is little correlation between the 95% credible interval endpoints and the amount of production history used in cases in which linear flow regime exists.

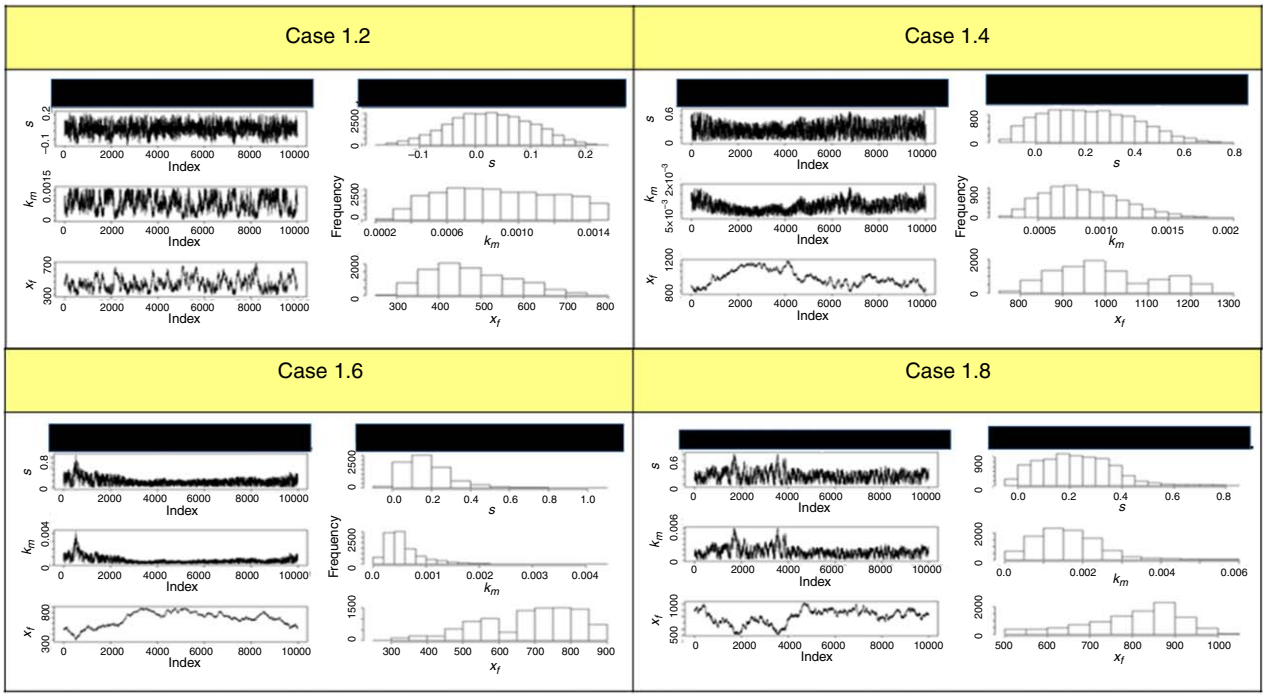

Fig. 6—ABC traceplot and histogram/density plot of even cases, Scenario 1 (number of iterations = 10,000).

Production Time	Case 1.2: $k_m = 0.0005$; md, $x_f = 500$ ft; $s = 0$								
	k_m – Posterior Distribution (md)			x_f – Posterior Distribution (ft)			s – Posterior Distribution		
	P2.5	P50	P97.5	P2.5	P50	P97.5	P2.5	P50	P97.5
1 year	Linear flow regime does not clearly develop within 1 year								
2 years	0.0002	0.0006	0.0010	231	507	796	−0.07	0.01	0.09
5 years	0.0002	0.0005	0.0010	363	547	765	−0.07	0.01	0.09
10 years	0.0002	0.0005	0.0010	383	543	848	−0.05	0.02	0.11
15 years	0.0004	0.0007	0.0010	384	515	661	−0.06	0.05	0.18
20 years	0.0003	0.0008	0.0010	398	489	815	−0.07	0.01	0.10

Table 7—95% credible intervals of model parameters as a function of production history used in the analysis.

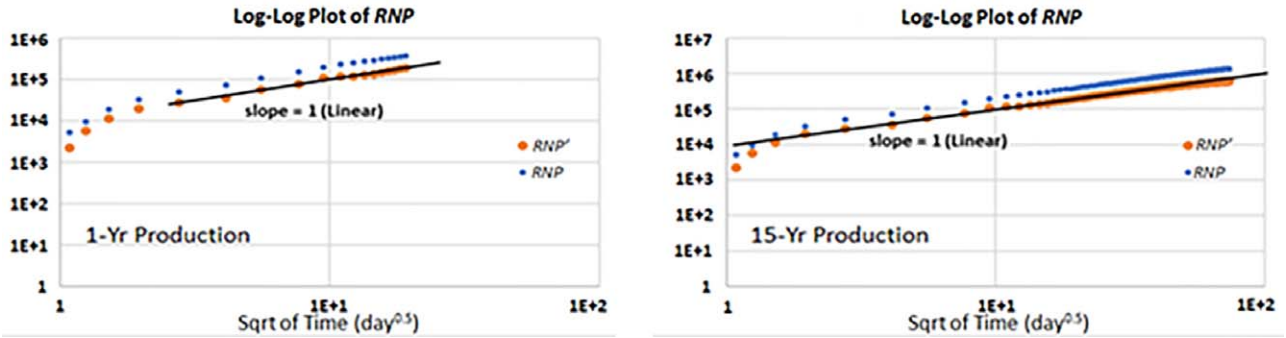

Fig. 7—Comparison of *RNP* and *RNP′* plots for 1- and 15-year production history.

Sensitivity to the Choice of Prior Distributions. One drawback of the Bayesian method is the potentially subjective choice of the prior distributions. Assumed priors can impact parameters' posteriors to a significant degree (this impact is modulated by the likelihood function). If the prior distribution places nontrivial probability mass on sets of parameter values that are distinct from those parameters' actual values within the data-generating mechanism (or—in the most extreme case—if the prior puts no density at all on the actual value), the posterior distribution can yield biased estimates of those parameters, especially when the likelihood function is not tightly concentrated around the actual values. On the other hand, when analysts attempt to evade this problem by using noninformative prior distributions that presume very little is known about the parameters' values *a priori*, the resulting posterior distributions will often contain a great deal of imprecision. Moreover, these noninformative priors can precipitate other challenges in the model-fitting process such as unnecessarily long computational times and multimodal posterior distributions. Therefore, the aim of this section is to understand how our choice of prior distribution affects the estimated posterior distributions for k_m, x_f, and s. The prior distribution of matrix permeability and fracture half-length are varied one at a time to clearly observe their impact. At first, the prior distribution of matrix permeability is fixed as a uniform distribution with a range from 0.0001 to 0.006 md, but the prior distribution of fracture half-length was varied both in range and shape as illustrated in Cases 1.1.1 through 1.1.4 of **Table 8.** The prior distribution of matrix permeability was varied in Cases 1.1.5 through 1.1.7 of Table 8. The results for each case report somewhat-dissimilar 95% credible intervals for the parameters as shown in Table 8. Notwithstanding, most of the 95% credible intervals contain the true values of the parameters except for some of the parameters in Cases 1.1.5, 1.1.6, and 1.1.7.

			Case 1.1: $k_m = 0.005$ md; $x_f = 500$ ft; $s = 0$								
	Prior Distribution	Prior Distribution	k_m – Posterior Distribution (md)			x_f – Posterior Distribution (ft)			s – Posterior Distribution		
Case	(k_m)	(x_f)	P2.5	P50	P97.5	P2.5	P50	P97.5	P2.5	P50	P97.5
1.1.1	$U(0.0001, 0.006)$	$N(500, 1^2)$	0.0046	0.0055	0.0060	464	492	529	−0.12	−0.07	0.01
1.1.2	$U(0.0001, 0.006)$	$N(500, 10^2)$	0.0013	0.0035	0.0054	367	577	965	−0.07	0.05	0.20
1.1.3	$U(0.0001, 0.006)$	$N(500, 50^2)$	0.0012	0.0036	0.0058	498	685	1,183	−0.07	0.00	0.08
1.1.4	$U(0.0001, 0.006)$	$U(0, 1{,}000)$	0.0017	0.0041	0.0058	467	688	954	−0.13	0.02	0.19
1.1.5	$U(0.0001, 0.1)$	$N(500, 10^2)$	0.0095	0.0513	0.0962	125	194	466	−0.91	0.25	1.72
1.1.6	$U(0.0001, 0.001)$	$N(500, 10^2)$	0.0004	0.0008	0.0010	515	766	878	−0.19	−0.11	−0.01
1.1.7	$LN(0.005, 0.001^2)$	$N(500, 10^2)$	0.0070	0.0236	0.0426	189	261	481	−0.16	0.00	0.14

LN = log-normal distribution

Table 8—95% credible interval of model parameters in each prior distribution.

Cases 1.1.1 through 1.1.3 test how the informativeness of the prior on x_f influences the marginal posterior distributions. In Case 1.1.1, the high precision of the prior on x_f results in concentrated posterior distributions for all the model parameters; in particular, the 95% prediction interval for k_m is tightly centered around the true value of 0.005 md. The 95% credible intervals of Case 1.1.1 are $k_m \varepsilon$ (0.0046 md, 0.006 md), $x_f \varepsilon$ (464, 529), and $s \varepsilon$ (−0.12, 0.01), respectively. In Cases 1.1.2 and 1.1.3, the prior standard deviation of x_f was increased to 10 and 50 ft, respectively. This implies that Case 1.1.3 was relatively uninformative. With this wide distribution, the posterior distributions still bracketed the true values for x_f, k_m, and s. Therefore, changing the standard deviation of the x_f distribution (within reasonable limits) did not superficially have much effect on the posterior distribution except in widening its credible interval. In Case 1.1.4, the x_f prior was assumed to be a uniform distribution with an interval of between 0 and 1,000 ft. The posterior for this case also bracketed the true value albeit with a spread roughly on par with that of case 1.1.2. The change in shape of the prior distribution also did not have much effect on the posterior distribution especially when compared to Case 1.1.3.

In Cases 1.1.5 through 1.1.7, the x_f prior distribution was fixed, whereas the k_m prior distribution was varied. The unusual and unrealistic large range on k_m in Case 1.1.5 results in marginal posterior distribution for x_f and k_m that did not encompass the true value (note, however, that the 97.5th percentile was close to true value of 500 ft). In Case 1.1.6, the prior uniform distribution for k_m did not contain the true value. As expected, the marginal posterior distributions for k_m, x_f, and s did not encompass the true value. Again and interestingly, even though the 95% credible interval for x_f and s for Case 1.1.6 did not encompass the true values, the interval endpoints were, once again, close. In Case 1.1.7, the prior log-normal distribution of k_m was centered at $e^{0.005+0.001^2/2} \approx 1.005$ with a standard deviation of $\sqrt{\left(e^{0.001^2}-1\right)*e^{2*0.005+0.001^2}} \approx 0.001$. As a result, the posterior distribution did not encompass the true input value. One interesting observation is that Case 1.1.6 was intentionally given the wrong matrix permeability prior distribution, whereas the matrix permeability prior distribution for Case 1.1.2 encompassed the true value. The resulting marginal posterior distributions for both cases are quite different, but upon history matching, both cases provided a good fit to the data. This is possibly evidence of model nonidentifiability, which often occurs in curve-fitting or inverse problems with multiple parameters. It suggests that the results from this type of analysis should be viewed with skepticism to the extent they do not agree with the engineer's understanding of reality. Overall, it can be concluded that the moderately concentrated prior distributions—distributions that account for the problem's engineering context—are useful for generating posterior credible intervals that contain the true value without unreasonably widening the interval. Insensible prior distributions for k_m and/or x_f can result in posterior distributions that all but exclude the true value of k_m, x_f, and s. Therefore, it is essential to use reality-informed prior distributions. In addition, it must be stated that the results from this methodology (as in any inverse problem) can be nonunique. This can be mitigated by eliminating potential solutions using information from other domains. Finally, the type/shape of prior distribution such as normal, log-normal, or uniform had little impact on the 95% credible interval in the cases studied, except in scenarios where the prior distribution put zero density on the true parameter value.

Sensitivity to the Number of Iterations Used. The n_{rec} argument in the ABC with MCMC algorithm is varied to understand the impact of the number of iterations on the marginal posterior distributions of model parameters (k_m, x_f, and s). The n_{rec} is a positive integer equal to the desired number of sampled points along the Markov chain. In theory, using a higher number of iterations during the MCMC process should aid convergence. An insufficient number of iterations can lead to unreliable posterior summaries because the

chains have not converged to their stationary distributions yet. However, the use of unnecessarily large number of iterations expends superfluous computational time without improving the posterior summaries. Thus, the challenge in this section is to determine the optimal number of iterations; ideally, we wish to achieve accurate posterior distributions at practical computational costs. **Table 9** presents 95% credible intervals for various iteration numbers. The posterior median (P50) and the width of each interval remain roughly similar for each parameter across iteration sizes. The computational time for generating 10,000 samples is fast—only 0.267 minutes. Increasing the number of iterations to 100,000 increases the computational time by a factor of about 10 (2.836 minutes). Further increasing the number of iterations to 10^6 leads to a computational time of 61.426 minutes. An examination of the trace plots for both 10,000 and 100,000 iterations show that both chains do not show evidence of nonconvergence. Accordingly, in this work, we have used 10,000 iterations for the rest of the analysis.

		Case 1.1: $k_m = 0.005$ md; $x_f = 500$ ft; $s = 0$								
Iteration Number	CPU Time (minutes)	k_m – Posterior Distribution (md)			x_f – Posterior Distribution (ft)			s – Posterior Distribution		
		P2.5	P50	P97.5	P2.5	P50	P97.5	P2.5	P50	P97.5
100	0.016	0.0035	0.0051	0.0059	455	535	639	−0.11	−0.04	0.07
1,000	0.041	0.0020	0.0035	0.0059	476	735	869	−0.11	−0.04	0.09
10,000	0.267	0.0013	0.0035	0.0054	367	577	965	−0.07	0.05	0.20
100,000	2.836	0.0020	0.0042	0.0059	476	643	867	−0.10	0.00	0.12
1,000,000	61.426	0.0021	0.0042	0.0059	484	634	861	−0.09	0.00	0.10

Table 9—95% credible intervals of model parameters in each iteration number.

Sensitivity to Tolerance Level τ. As described previously, the Marjoram version of ABC-MCMC can select an appropriate threshold $\omega_{\max}$ for what constitutes data simulated from the likelihood that is sufficiently close to the observed data. This feature of the algorithm removes some of the subjectivity involved, but not all of it, because the user must still specify a quantile tolerance level τ. We now consider the effect of varying that tolerance level between 0.001 on the low end and 0.9 on the high end. **Table 10** presents the 95% credible intervals that result from this sensitivity analysis for 100,000 iterations. Overall, we recommend using a tolerance of 0.001 for these data which, unsurprisingly, results in the lowest $\omega_{\max}$ of all the choices studied. This recommendation is based on the observation that computational time was not greatly inflated by this more rigorous setting.

		Case 1.1: $k_m = 0.005$; md, $x_f = 500$ ft; $s = 0$								
τ	CPU Time (minutes)	k_m – Posterior Distribution (md)			x_f – Posterior Distribution (ft)			s – Posterior Distribution		
		P2.5	P50	P97.5	P2.5	P50	P97.5	P2.5	P50	P97.5
0.001	2.604	0.0017	0.0038	0.0055	368	479	717	−0.02	0.01	0.04
0.01	2.193	0.0021	0.0042	0.0056	397	648	841	−0.03	0.11	0.33
0.1	2.239	0.0019	0.0041	0.0056	359	651	840	−1.66	−0.10	1.05
0.5	2.402	0.0018	0.0041	0.0056	257	536	815	−5.44	−0.30	4.88
0.8	2.321	0.0015	0.0036	0.0054	208	541	818	−6.99	−0.09	6.89
0.9	2.267	0.0012	0.0033	0.0053	252	595	832	−7.30	−0.05	7.24

Table 10—95% credible intervals of model parameters for varied ABC-MCMC tolerances.

As a result of these sensitivity analysis cases, we will use the following algorithm tuning parameters going forward:

1. Use at least 2 years of production history in our analysis.
2. Assume symmetric, relatively concentrated prior distributions.
3. Set the number of iterations in the ABC-MCMC chain to 10,000.
4. $\tau = 0.001$ for ABC-MCMC samplers of the Marjoram type.

Scenario 2—Impact of Hydraulic Fracturing Fluid on the Estimation Accuracy of the RTA-ABC Methodology. Field data from Marcellus Shale in northeastern West Virginia indicated that approximately 2 to 26% of the fracture fluid is recovered during flowback (Zhou et al. 2015). This fact may initially and materially affect well productivity. Therefore, study on the impact of hydraulic fracturing fluid flowback on our RTA-ABC methodology is considered. To generate synthetic production data to study the fracturing fluid flowback effect, a horizontal water injector is created in the same location as the horizontal producer in the reservoir simulator. Volumes of water equal to one fracture-system volume are injected into the fracture system. After the injected fluids are in place, the horizontal water injector is shut in or turned off, and the horizontal producer is turned on. A Corey-type relative permeability relationship is assumed for multiphase flow in the fractures. A homogeneous reservoir with five fracture stages in a horizontal well completion is considered and modeled with the reservoir model. Production data were generated for 20 years. A sensitivity analysis is shown in **Table 11** (Cases 2.1 to 2.4 of Table 5). RNP and derivative RNP plots for scenarios that include fracture fluid flowback are like those generated for scenarios in which fracture fluid flowback is not considered. This is except for the early time data (roughly first 8 hours of production) in which multiphase flow of water and gas results in nonlinearity in the RNP and derivative RNP plot as shown in the middle and right-most plots of **Fig. 8.** For estimation, we still used the single-phase flow equation because of very low water production during linear flow regime. We can see that the probabilistic range (95% credible interval) from our method encompassed the true values in all

cases. However, we could detect linear flow and use our analysis procedure only after 30 days for the 0.005 md cases and after 1 year of production for the 0.0005-md cases. This essentially implies that the engineer will have to wait longer to be able to characterize fracture and reservoir properties, especially for ultralow permeabilities.

				Fracturing Fluid Flowback Impact; $s = 0$								
				k_m – Posterior Distribution (md)			x_f – Posterior Distribution (ft)			s – Posterior Distribution		
Scenario 2	k_m (md)	x_f (ft)	n_f	P2.5	P50	P97.5	P2.5	P50	P97.5	P2.5	P50	P97.5
Case 2.1	0.005	500	5	0.0009	0.0032	0.0058	354	530	1,007	−0.06	−0.01	0.03
Case 2.2	0.0005	500	5	0.0003	0.0011	0.0019	232	354	727	−0.05	0.32	0.96
Case 2.3	0.005	900	5	0.0021	0.0043	0.0059	619	822	1,139	−0.08	0.00	0.08
Case 2.4	0.0005	900	5	0.0006	0.0014	0.0020	560	742	1,131	−0.16	0.14	0.52

Table 11—95% credible intervals of model parameters in fracturing fluid flowback scenarios.

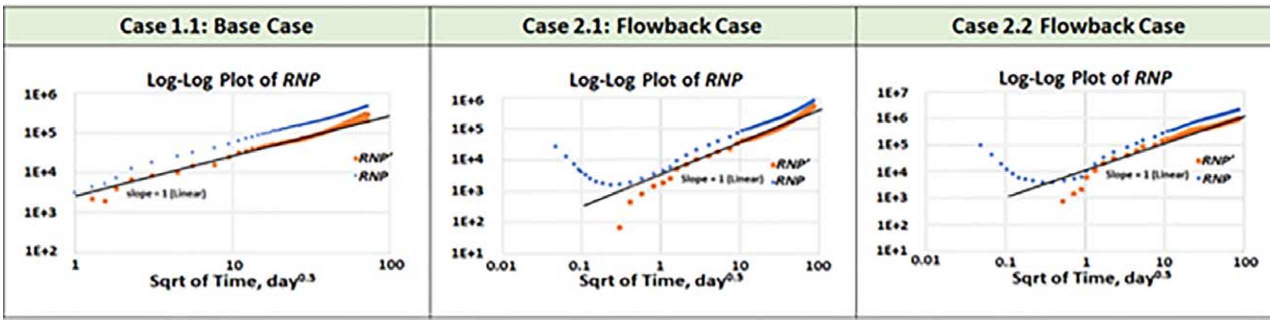

Fig. 8—Comparison of *RNP* and *RNP′* plots with and without flowback.

Scenario 3—Impact of Finite Fracture Conductivity on the Estimation Accuracy of the RTA-ABC Methodology. **Table 12** presents the results after the RTA-ABC methodology has been applied to Cases 3.1 to 3.4 of Table 5. In this section, a five-stage horizontal well completion was modeled in a reservoir simulator. For example, in Case 3.1, Stages 1, 3, and 5 have finite permeability of 1.5 md, whereas Fracture Stages 2 and 4 are infinitely conductive. Cases 3.2 to 3.4 can be described in the same manner. The results encompass the true reservoir model input values except for skin factor in all the four scenarios. The 95% credible interval for skin was a positive value between 0.04 and 0.61, which narrowly missed the true skin value of 0. Focusing on Case 3.1 to illustrate the results, the 95% credible intervals are k_m ε (0.0004 md, 0.001 md), x_{f1} ε (421, 737), and s ε (0.04, 0.61), respectively. We also observe that the estimated total skin in Case 3.1 (finite fracture conductivity case) is higher than for Case 1.2 (infinite fracture conductivity case). This is because of the impact of apparent skin caused by the finite fracture conductivity and converging flow (Cinco-Ley and Samaniego-V. 1981). In addition, in the finite conductivity cases, the linear flow regime occurs later compared to the infinite conductivity cases (10 days vs. 1,000 days). Accordingly, to be able to characterize the reservoir earlier, the RTA portion of our workflow needs to be replaced with a model that can be used to estimate reservoir parameters during bilinear flow.

					Finite Fracture Conductivity Impact; $s = 0$								
					k_m – Posterior Distribution (md)			x_f – Posterior Distribution (ft)			s – Posterior Distribution		
Scenario 3	k_m (md)	x_f (ft)	n_f	Finite Fracture	P2.5	P50	P97.5	P2.5	P50	P97.5	P2.5	P50	P97.5
Case 3.1	0.0005	500	5	1, 3, 5	0.0004	0.0008	0.0010	421	546	737	0.04	0.24	0.41
Case 3.2	0.0005	500	5	2, 4	0.0003	0.0007	0.0010	453	588	869	0.07	0.20	0.40
Case 3.3	0.0005	900	5	1, 3, 5	0.0003	0.0007	0.0010	680	892	1,252	0.03	0.16	0.35
Case 3.4	0.0005	900	5	2, 4	0.0004	0.0007	0.0010	671	908	1,138	0.00	0.13	0.31

Table 12—95% credible intervals of model parameters in finite conductivity effect.

Scenario 4—Impact of Fracture Half-Length Heterogeneity on the Estimation Accuracy of the RTA-ABC Methodology. The effect of fracture heterogeneity is investigated by building and generating data from a reservoir model that contains two sets of equally sized fractures. In this scenario, Fractures 1, 3, and 5 are 900 ft long, whereas Fractures 2 and 4 are 500 ft long. Four scenarios are investigated here as shown in **Table 13.** Fracture permeability in the finite conductivity case is 1.5 md. The RTA-Bayesian (ABC) methodology is again applied to the synthetically generated data, albeit with a modification in cross-sectional area (A_c) which is defined as shown in Eq. 10.

$$A_c = 4h(x_{f1}n_{f1} + x_{f2}n_{f2}). \quad (10)$$

Similar to the finite fracture conductivity section, the onset of the linear flow regime in Case 4.3 (which has both finite and infinite fracture conductivity fractures) occurs after 1,000 days—which is a lot later than for the infinite conducivity fracture system. Table 13 presents the results after the RTA-ABC methodology has been applied to Cases 4.1 through 4.4 of Table 5. The 95% credible intervals, for example in Case 4.1, are $k_m \in$ (0.0003 md, 0.001 md), $x_{f1} \in$ (570, 1,256), $x_{f2} \in$ (184, 872), and $s \in (-0.03, 0.24)$, respectively. The intervals encompass the true values except for the skin parameter in Case 4.4. Again, the estimated skin value at 0.43 (P97.5) in Case 4.4 is not very different from the true value at zero skin.

					Heterogeneity of x_f Impact											
								Posterior Distribution (ft)								
					k_m – Posterior Distribution (md)			x_{f1}			x_{f2}			s – Posterior Distribution		
Case	k_m (md)	x_f (ft)	n_f	Finite Fracture	P2.5	P50	P97.5	P2.5	P50	P97.5	P2.5	P50	P97.5	P2.5	P50	P97.5
Case 4.1	5×10^{-4}	900 and 500	3 and 2	Infinite	3×10^{-4}	7×10^{-4}	1×10^{-3}	570	955	1,256	184	627	872	−0.03	0.09	0.24
Case 4.2	5×10^{-4}	900 and 500	2 and 3	Infinite	4×10^{-4}	7×10^{-4}	1×10^{-3}	551	999	1,268	195	567	862	−0.04	0.11	0.30
Case 4.3	5×10^{-4}	900 and 500	3 and 2	Finite in $x_f = 500$ ft with 1.5 md	4×10^{-4}	7×10^{-4}	1×10^{-3}	568	942	1,265	150	491	853	−0.01	0.11	0.28
Case 4.4	5×10^{-4}	900 and 500	3 and 2	Finite in $x_f = 900$ ft with 1.5 md	4×10^{-4}	7×10^{-4}	1×10^{-3}	560	960	1,268	165	622	865	0.12	0.25	0.43

Table 13—95% credible intervals of model parameters in fracture half-length heterogeneity effect.

Application of RTA-ABC Methodology to a Field Case. In this section, the RTA-Bayesian (ABC) method is applied to actual field data for further validation. The field production data of Well A from Barnett Shale is from the work of Bello and Wattenbarger (2010). The production and pressure profiles are presented in **Fig. 9.** The rock/fluid properties and completion parameters are presented in **Table 14.** The field data are analyzed using the procedure of Bello and Wattenbarger (2010). The log-log plot of RNP against square root of time is established to check for a unit slope (linear flow regime) in **Fig. 10** with the assumption of constant p_{wf}. Next, a line is drawn through the origin passing through the linear zone on the plot of RNP against square root of time **(Fig. 11).** The slope (m) of this line is determined as 64,000 psi^2-D$^{0.5}$/cp^{-1}-Mscf^{-1}. According to Eq. 4, the slope (m) between RNP and the square root of time is equal to $\frac{1{,}262T}{\sqrt{k_m(\phi\mu c_t)_i}A_c}$. Therefore, the matrix permeability (k_m) can be calculated if A_c (matrix-fracture surface area) is known. The calculated k_m from the methodology of Bello and Wattenbarger (2010) is $k_m = \left(\frac{1{,}262T}{\sqrt{(\phi\mu c_t)_i}A_c m}\right)^2 = \left[\frac{1{,}262(175 + 460)}{\sqrt{(0.034)(0.0199)(0.000303)}(4.03{*}10^6)(64000)}\right]^2 = 0.000047$ md. This is the deterministic result. Next, the RTA-Bayesian (ABC) method is applied to the same field data. In **Fig. 12,** the RNP is first plotted against the square root of superposition time to identify linear flow regime for a variable production rate case. Superposition time here refers to the finite summation term in Eq. 7. The line is clearly exhibited with a unit slope after the square root of superposition time is larger than 10 day$^{0.5}$. For the second step, Eq. 7 is used for defining the relationship between the observed data and the simulated data. Eq. 8 again provides the likelihood assumption for ε. Next, the range of the prior distributions are chosen to reflect prior knowledge about the reservoir. The matrix permeability is in the range of 0.00001 to 0.001 md from a literature review (Parshall 2008). The mean of fracture half-length is assigned as 1,700 ft according to Well A's completion data in Table 14. The original Marjoram version of ABC-MCMC is attempted with maximum distance ($\omega_{\max}$) between observed data and simulated data set to 0.01. Parameter draws are taken from the approximate marginal posterior distributions; their results are summarized in **Table 15.** The 95% credible intervals are $k_m \in$ (0.00003 md, 0.00006 md), $x_f \in$ (1,710 ft, 1,713 ft), and $s \in (-0.0014, 0.0041)$, respectively. The calculated probabilistic parameters agree with the analytical solution from the procedure of Bello and Wattenbarger (2010; k_m, s, and x_f; Table 15). The skin estimate's 95% credible interval is from −0.0014 to 0.0041, which is close to the true value of zero skin. **Fig. 13** shows the prior distributions, trace plots, posterior distributions, smoothed empirical cumulative distribution function plots, and Euclidean plots for the field case. The posterior distributions are different from the imposed priors. Evidence of sampling convergence is unambiguously observed in the trace plots and by the conical shape of Euclidean plots for skin and matrix permeability. The results are converged nearly to the point of zero Euclidean distance. The plots indicate a convergence problem for x_f, which probably accounts for this parameter's narrow 95% credible interval (1,710 to 1,713 ft). Notwithstanding, it is comforting that the parameters' P50 point estimates align with the results of the approach of Bello and Wattenbarger (2010). This agreement between the two methods supports the hypothesis that engineers can rely upon RTA-Bayesian (ABC) methodology to characterize reservoir properties with acceptable accuracy. Also, **Fig. 14** shows that there is agreement between the fitted and actual RNP data. The fitted RNP data were taken from the posterior 50th percentile and 95% credible interval of the RTA-ABC analysis.

As discussed previously, one could argue that the model should be parameterized by fracture half-length times the square root of permeability instead of by each parameter independently. We reran the analysis under this alternate parameterization to address such a concern; the results are shown in **Fig. 15 and Table 16.**

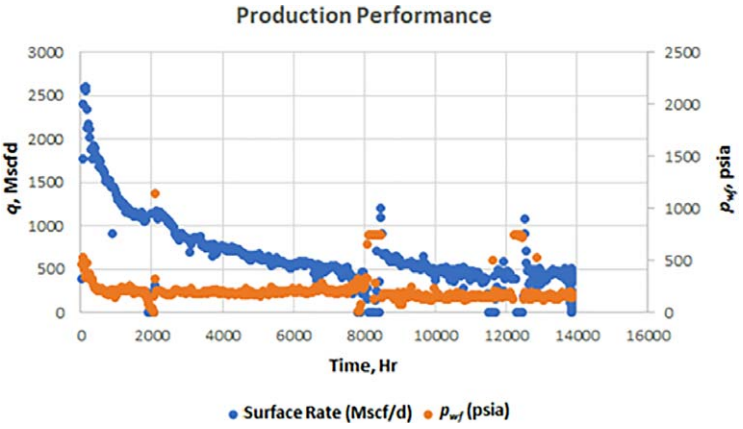

Fig. 9—Well A production and pressure profile with pressure.

Well A					
Rock Properties		Fluid Properties		Completion Parameters	
Reservoir thickness	140 ft	SG	0.65	$2x_f$	3,417 ft
Calculated matrix permeability	0.00005 md	B_{gi}	0.00535 rcf/scf	$A_c = (4x_f h)n_f$	4.03×10^{-6} ft^2
Porosity	0.034	c_t	0.000303 psi^{-1}		
		μ_i	0.0199 cp		
		p_i	3,000 psi		
		T	175°F		

Table 14—Well A rock/fluid properties and completion parameters. SG = specific gravity.

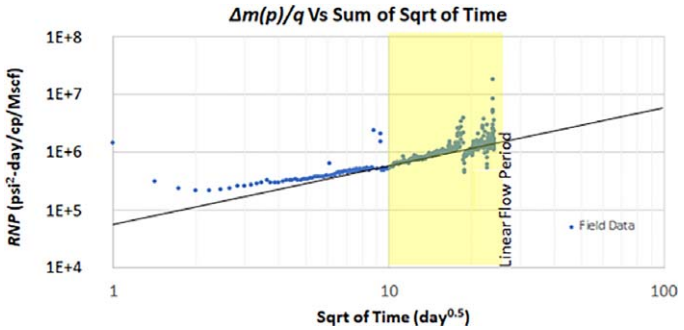

Fig. 10—Log-log *RNP* plot against square root of time for Well A based on Bello and Wattenbarger (2010).

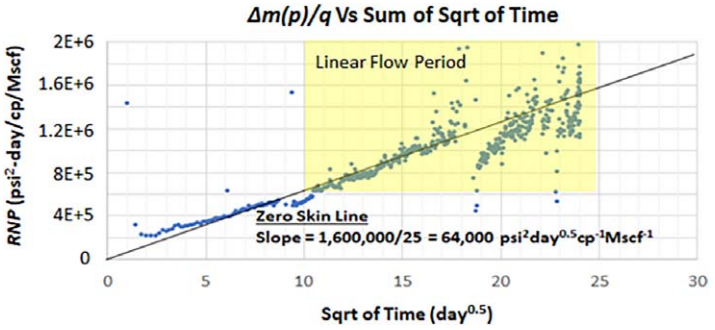

Fig. 11—*RNP* plot against square root of time for Well A based on the work of Bello and Wattenbarger (2010).

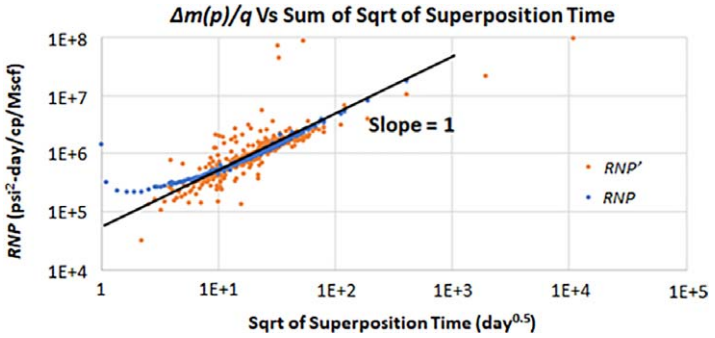

Fig. 12—Log-log *RNP* plot against square root of superposition time for Well A.

	Posterior Distribution			Deterministic Results from Approach of Bello and Wattenbarger (2010)
Well A	P2.5	P50	P97.5	
k_m (md)	0.00003	0.00005	0.00006	0.00005
x_f (ft)	1,710	1,712	1,713	1,709
s	−0.0014	0.0014	0.0041	0

Table 15—95% credible intervals of model parameters in Well A.

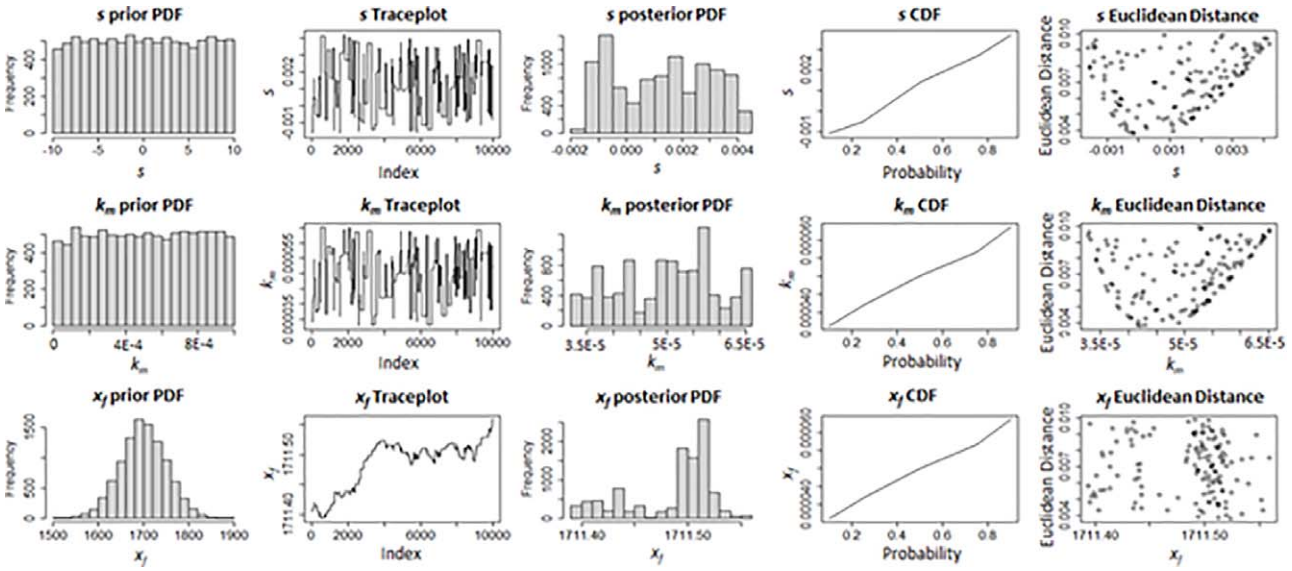

Fig. 13—Prior distributions, trace plots, posterior probability distribution function (PDF) plots, cumulative distribution function (CDF) plots, and Euclidean plots for the field case (Well A).

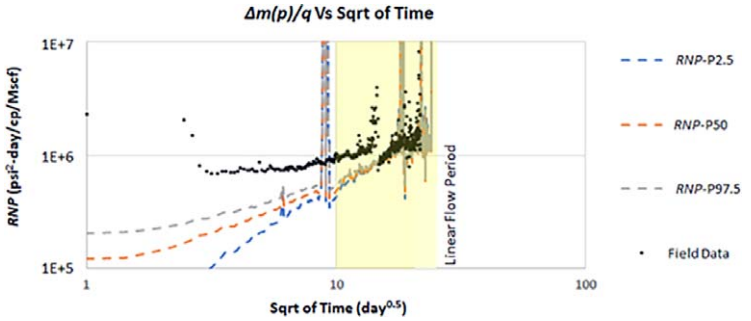

Fig. 14—*RNP* plot for the field case showing agreement between prediction using RTA and ABC-MCMC and actual Well A data.

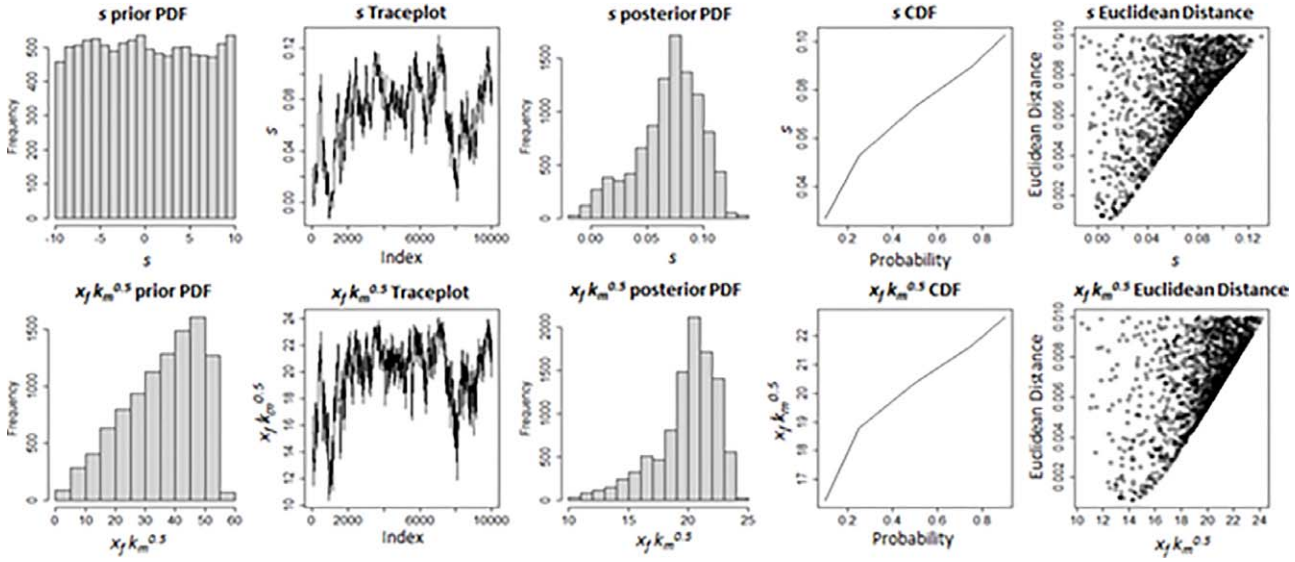

Fig. 15—Trace plots, PDF plots, CDF plots, and Euclidean plots for the field case (Well A) using the fracture-half-length and square root of permeability product.

	Posterior Distribution			Deterministic Results from Approach of Bello and Wattenbarger (2010)
Well A	P2.5	P50	P97.5	
$x_f\sqrt{k_m}$ (ft-md$^{0.5}$)	16.28	20.38	22.67	20.92
s	0.02	0.07	0.11	0

Table 16—95% credible intervals of model parameters in Well A.

Conclusions

- Moderately concentrated prior distributions were valuable for accurate and well calibrated estimation of the model parameters' posterior distributions (k_m, x_f, s). Such accuracy and calibration are reflected in the fact that the 95% credible intervals encompassed the deterministic true values in most scenarios in which such a prior was used.
- Analysis in ultratight gas reservoirs required at least 1 year of production data because the linear flow regime, which is important for the RTA method to characterize reservoir/wellbore parameters, was only clearly observed after 1 year of production. There was also no strong correlation between the accuracy of prediction intervals and the amount of production history used.
- The results showed that at least 10,000 runs are required for samples' distributions to converge to their target posteriors. However, more than a million runs are not recommended because of unnecessarily long computational times required.
- The RTA-ABC algorithm functioned well with synthetic production data from a variety of complex reservoir cases. The 95% credible intervals encompassed the true values of the simulation model parameters k_m and x_f in most cases, and s in some cases. This is because there was an additional skin (such as choked skin) created in the system, especially in the finite fracture conductivity cases. However, the estimated skin credible intervals were so narrow and near the true value that the intervals' maximum deviation from the true value of skin (i.e., zero) would not materially affect any type of engineering analysis.
- The presence of hydraulic fracturing fluid in the fractures meant that we could not use the RTA-ABC technique for early time data. This was because flowback is significant mostly at the initial stage of production. For long-term production analysis (greater than 6 months to 1 year), the RTA-Bayesian (ABC) was feasible for reservoir characterization.
- For the scenarios including finite-conductivity fractures, bilinear flow (slope = 0.25) dominated the production data trends at the initial stage. As such, bilinear flow coupled with wellbore storage can be dominant for a long time before linear flow is observed. Thus, for low-permeability reservoirs, the production must be of sufficient extent to ensure that the linear flow regime is observed. Otherwise, the RTA-Bayesian (ABC) analysis will not be practicable.
- The impact of heterogeneity on fracture half-length can be handled by adjusting the cross-sectional area equation. The RTA-Bayesian (ABC) credible intervals encompassed the true parameter values for these scenarios.
- Finally, for the single real production data set considered in this work, the 95% credible intervals of matrix permeability and fracture half-length were similar to the results obtained by Bello and Wattenbarger (2010).

Possible future extensions of this work might investigate the use of other Bayesian sampling algorithms such as adaptive or Hamiltonian Monte Carlo methods, both alone and in conjunction with ABC. Also, future investigations might compare more complicated forms of the likelihood-intensive MCMC algorithms to their approximate equivalents. Such research might further improve computational time and/or estimation accuracy.

Also, the use of this methodology can be expanded upon in future work to include the characterization of the other petrophysical properties such as porosity and thickness and to consider more robust RTA alternatives. Finally, the prior standard deviation of 10 ft for fracture half-length (in Table 3) was assumed to be large enough to encompass the range of uncertainty associated with a mean of 500 or 900 ft. We acknowledge that the results could change with a different prior standard deviation—or a differently shaped prior altogether—(although the sensitivity analysis reported in Table 8 does not provide substantial reason to think so), and we propose further investigating the effect of these assumptions in future work.

Nomenclature

A_c = cross-sectional area perpendicular to flow, ft^2, L^2
c_t = total compressibility, $psi^{-1}, m^{-1}Lt^2$
D_D = dimensionless drawdown
f_{cp} = correction factor
h = reservoir thickness, ft, L
i = subscript i anywhere implies initial reservoir conditions
k_m = matrix permeability, md, L^2
$l(X|\theta)$ = likelihood function
$m(p_i)$ = initial gas pseudopressure, $\frac{psi^2\text{-D}}{cp\text{-Mscf}}, mL^{-4}t^{-4}$
$m(p_{wf})$ = bottomhole flowing gas pseudopressure, $\frac{psi^2\text{-D}}{cp\text{-Mscf}}, mL^{-4}t^{-4}$
q = gas-flow rate, $Mscf/D, \frac{L^3}{t}$
q_j = gas-flow rate at time j, $Mscf/D, \frac{L^3}{t}$
q_n = last recorded gas-flow rate, which should be nonzero
n_f = number of hydraulic fractures
s = skin factor
T = reservoir temperature, °F, T
x_f = fracture half-length ft, L
ε = aleatory error
μ = gas viscosity, cp, $mL^{-1}t^{-1}$
μ_m = RNP from the numerical simulator, $\frac{psi^2\text{-D}}{cp\text{-Mscf}^2}, mL^{-7}t^{-5}$
$\pi(X)$ = constant in θ
$\pi(\theta)$ = prior probability distribution of model parameters
$\pi(\theta|X)$ = posterior distribution of parameters θ (which may be a vector), given observed data X
ϕ = reservoir porosity

References

Anderson, D. M., Nobakht, M., Moghadam, S. et al. 2010. Analysis of Production Data from Fractured Shale Gas Wells. Paper presented at the SPE Unconventional Gas Conference, Pittsburgh, Pennsylvania, USA, 23–25 May. SPE-131787-MS. https://doi.org/10.2118/131787-MS.

Beaumont, M. A., Zhang, W., and Balding, D. J. 2002. Approximate Bayesian Computation in Population Genetics. *Genetics* **162** (4): 2025–2035. https://doi.org/10.1093/genetics/162.4.2025.

Bello, R. O. and Wattenbarger, R. A. 2010. Multi-Stage Hydraulically Fractured Horizontal Shale Gas Well Rate Transient Analysis. Paper presented at the North Africa Technical Conference and Exhibition, Cairo, Egypt, 14–17 February. SPE-126754-MS. https://doi.org/10.2118/126754-MS.

Blasingame, T. A. 2013. P663 Formation Evaluation and Analysis of Reservoir Performance Handout, Texas A&M. Class of 2013, https://www.scribd.com/document/332188117/P663-Blasingame-PA-v20130722-pdf (accessed 15 February 2019).

Chen, C., Li, R., Gao, G. et al. 2016. EUR Assessment of Unconventional Assets Using Parallelized History Matching Workflow Together with RML Method. Paper presented at the SPE/AAPG/SEG Unconventional Resources Technology Conference, San Antonio, Texas, USA, 1–3 August. URTEC-2429986-MS. https://doi.org/10.15530/URTEC-2016-2429986.

Cinco-Ley, H. and Samaniego-V., F. 1981. Transient Pressure Analysis on Fractured Wells. *J Pet Technol* **33** (9): 1749–1766. SPE-7490-PA. https://doi.org/10.2118/7490-PA.

De Holanda, R. W. 2019. *Material Balance Reservoir Models Derived from Production Data*. PhD dissertation, Texas A&M University, College Station, Texas, USA (May 2019).

Gelman, A. and Rubin, D. 1992. Inference from Iterative Simulation Using Multiple Sequences. *Stat Sci* **7** (4): 457–472. https://doi.org/10.1214/ss/1177011136.

Gong, X., Gonzalez, R. A., McVay, D. et al. 2011. Bayesian Probabilistic Decline-Curve Analysis Reliably Quantifies Uncertainty in Shale-Well-Production Forecasts. Paper presented at the Canadian Unconventional Resources Conference, Calgary, Alberta, Canada, 15–17 November. SPE-147588-MS. https://doi.org/10.2118/147588-MS.

Goodwin, N. 2012. Bridging the Gap between Deterministic and Probabilistic Uncertainty Quantification Using Advanced Proxy Based Methods. Paper presented at the SPE Reservoir Simulation Symposium, Houston, Texas, USA, 23–25 February. SPE-173301-MS. https://doi.org/10.2118/173301-MS.

Guseo, R. and Dalla Valle, A. 2005. Oil and Gas Depletion: Diffusion Models and Forecasting under Strategic Intervention. *Stat Methods Appt* **14** (3): 375–387. https://doi.org/10.1007/s10260-005-0118-6.

Hartig, F., Calabrese, J. M., Reineking, B. et al. 2011. Statistical Inference for Stochastic Simulation Models: Theory and Application. *Ecol Lett* **14** (8): 816–827. https://doi.org/10.1111/j.1461-0248.2011.01640.x.

Ibrahim, M. H. and Wattenbarger, R. A. 2006. Analysis of Rate Dependence in Transient Linear Flowing Tight Gas Wells. Paper presented at the SPE Conference, Abu Dhabi, UAE, 5–8 November. SPE-100836-MS. https://doi.org/10.2118/100836-MS.

Jabot, F., Faure, T., Dumoulin, N. et al. 2015. EasyABC: A Package To Perform Efficient Approximate Bayesian Computation Sampling Schemes. In Cran.r Project, 30 June 2015. https://cran.r-project.org/web/packages/EasyABC/vignettes/EasyABC.pdf (accessed 15 February 2019).

Khanal, A., Khoshghadam, M., and Lee, W. J. 2016. Accurate Forecasting of Liquid Rich Gas Condensate Reservoirs with Multiphase Flow. Paper presented at the SPE/AAPG/SEG Unconventional Resources Technology Conference, San Antonio, Texas, USA, 1–3 August. URTEC-2426222-MS. https://doi.org/10.15530/URTEC-2016-2426222.

Komurcu, C. 2014. *Effect of Viscosity-Compressibility Product Variation on the Analysis of Fractured Well Performances in Tight Unconventional Reservoirs*. MS thesis, Colorado School of Mines, Golden, Colorado, USA.

Lintusaari, J., Gutmann, M. U., Dutta, R. et al. 2017. Fundamentals and Recent Developments in Approximate Bayesian Computational. *Syst Biol* **66** (1): e66–e82. https://doi.org/10.1093/sysbio/syw077.

Maria, G. 2004. A Review of Algorithms and Trends in Kinetic Model Identification for Chemical and Biochemical Systems. *Chem Biochem Eng Q* **18** (3): 195–222.

Marjoram, P., Molitor, J., Plagnol, V. et al. 2003. Markov Chain Monte Carlo without Likelihoods. *Proc Natl Acad Sci U S A* **100** (26): 15324–15328. https://doi.org/10.1073/pnas.0306899100.

Moinfar, A., Erdle, J. C., and Patel, K. 2016. Comparison of Numerical vs Analytical Models for EUR Calculation and Optimization in Unconventional Reservoirs. Paper presented at the SPE Low Perm Symposium, Denver, Colorado, USA, 5–6 May. SPE-180209-MS. https://doi.org/10.2118/180209-MS.

Nejadi, S., Leung, J. Y., Trivedi, J. J. et al. 2015. Integrated Characterization of Hydraulically Fractured Shale Gas Reservoirs Production History Matching. *SPE Res Eval & Eng* **18** (4): 481–494. SPE-171664-PA. https://doi.org/10.2118/171664-PA.

Nobakht, M. and Clarkson, C. R. 2012. A New Analytical Method for Analyzing Linear Flow in Tight/Shale Gas Reservoirs: Constant Rate Boundary Condition. *SPE Res Eval & Eng* **15** (1): 51–59. SPE-143990-PA. https://doi.org/10.2118/143990-PA.

Parshall, J. 2008. Barnett Shale Showcases Tight-Gas Development. *J Pet Technol* **60** (9): 48–55. SPE-0908-0048-JPT. https://doi.org/10.2118/0908-0048-JPT.

Paryani, M., Awoleke, O., Ahmadi, M. et al. 2017. Approximate Bayesian Computation for Probabilistic Decline-Curve Analysis in Unconventional Reservoirs. *SPE Res Eval & Eng* **20** (2): 478–485. SPE-183650-PA. https://doi.org/10.2118/183650-PA.

Pritchard, J., Seielstad, M., Perez-Lezaun, A. et al. 1999. Population Growth of Human Y Chromosomes: A Study of Y Chromosome Microsatellites. *Mol Biol Evol* **16** (12): 1791–1798. https://doi.org/10.1093/oxfordjournals.molbev.a026091.

Plummer, M. 2019. rjags: Bayesian Graphical Models Using MCMC. *R* package version 4-10. https://CRAN.R-project.org/package=rjags (accessed 15 July 2020).

R Core Team. 2020. *R: A Language and Environment for Statistical Computing*. Vienna, Austria: R Foundation for Statistical Computing. https://www.R-project.org/ (accessed 15 July 2020).

Sureshjani, M. H., Ahmadi, M., and Fahimpour, J. 2020. Uncertainty Quantification in Heterogeneous Tight/Shale Reservoirs from Analysis of Transient/Boundary-Dominated Production Data. *J Nat Gas Sci Eng* **79** (2020): 103342. https://doi.org/10.1016/j.jngse.2020.103342.

Wantawin, M., Wei, Y., Dachanuwattana, S. et al. 2017. An Iterative Response-Surface Methodology by Use of High-Degree-Polynomial Proxy Models for Integrated History Matching and Probabilistic Forecasting Applied to Shale-Gas Reservoirs. *SPE J*. **22** (6): 2012–2031. SPE-187938-PA. https://doi.org/10.2118/187938-PA.

Wegmann, D., Leuenberger, C., and Excoffier, L.. 2009. Efficient Approximate Bayesian Computation Coupled with Markov Chain Monde Carlo without Likelihood. *Genetics* **182** (4): 1207–1218. https://doi.org/10.1534/genetics.109.102509.

Yu, W., Tan, X., Zuo, L. et al. 2016. A New Probabilistic Approach for Uncertainty Quantification in Well Performance of Shale Gas Reservoirs. *SPE J*. **21** (6): 2038–2048. SPE-183651-PA. https://doi.org/10.2118/183651-PA.

Yuhun, P. 2019. *Using Rate Transient Analysis and Bayesian Algorithms for Reservoir Characterization in Hydraulically Fractured Gas Wells during Linear Flow*. MS thesis, University of Alaska, Fairbanks, Alaska, USA (May 2019).

Zagorski, W. A., Wrightstone, G. R., and Bowman, D. C. 2012. Appalachian Basin Marcellus Gas Play, AAPG Wiki. http://wiki.aapg.org/Appalachian_Basin_Marcellus_gas_play (accessed 15 February 2019).

Zhou, Q., Dilmore, R., Kleit, A. et al. 2015. Evaluating Fracturing Fluid Flowback in Marcellus Using Data Mining Technologies. Paper presented at the SPE Hydraulic Fracturing Technology Conference, The Woodlands, Texas, USA, 3–5 February. SPE-173364-MS. https://doi.org/10.2118/173364-MS.